Faculty of Aerospace Engineering

Effects of Structural Failures on the Safe Flight Envelope of Aircraft

A database approach to flight envelope prediction and protection

H. N. Nabi

August 23, 2016

TU Delft Delft University of Technology

Challenge the future

Effects of Structural Failures on the Safe Flight Envelope of Aircraft

A database approach to flight envelope prediction and protection

Master of Science Thesis

For obtaining the degree of Master of Science in Aerospace Engineering
at Delft University of Technology

H. N. Nabi

August 23, 2016

Faculty of Aerospace Engineering · Delft University of Technology

Delft University of Technology

Delft University Of Technology
Department Of
Control and Simulation

The undersigned hereby certify that they have read and recommend to the Faculty of Aerospace Engineering for acceptance a thesis entitled **"Effects of Structural Failures on the Safe Flight Envelope of Aircraft"** by **H. N. Nabi** in partial fulfillment of the requirements for the degree of **Master of Science**.

Dated: August 23, 2016

Readers:

dr.ir. Q. P. Chu

dr.ir. C. C. de Visser

dr.ir. E. van Kampen

dr.ir. Richard P. Dwight

Acknowledgments

I would like to begin by praising and paying my humble gratitude to the God Almighty. Blessings bestowed upon me by God Almighty are countless.

The research conducted in this MSc. thesis would not have been possible without the support and guidance of several individuals to whom I owe sincere gratitude and respect.

Firstly, I would like show my profound gratitude and appreciation to my daily supervisor Dr. Coen de Visser for his guidance throughout the course of this thesis. I greatly appreciate his invaluable insights and support that kept me motivated throughout the thesis. I would also like to thank Dr. Q. P. Chu for his support and supervision.

I would like to appreciate and acknowledge the help and assistance I received from Ye Zhang, Herman Koolstra and Menno Klassen.

I would like to thank my friends - Zohaib Saleem, Arif Pascal, Pulkit Goyal, Malik Doole, Mengyang Li, Nicolas Abuter, Waqas Hayat, Usman Ishfaq, Fahim Riaz, Usman Hasan, Halima Saroukh, Cristina Mendez and Daphne Rein-Weston. Furthermore, I would like to thank my friends in room 0.08.

I would also like to thank my friends back home specially the class of Aero-08 and Miss. Zainab Saleem who motivated me to join TU Delft.

Last, but certainly not the least, I would like to thank and show my utmost gratitude to my parents and my two lovely sisters, Sana Najmusehar and Sadia Sabahat, for their unconditional love, care and support. I dedicate this work to them.

Acronyms

C&S	Control & Simulation
CAST	Commercial Aviation Safety Team
CFD	Computational Fluid Dynamics
DUT	Delft University of Technology
FCC	Flight Control Computer
HJB	Hamilton Jacobi Bellman
HJI	Hamilton Jacobi Isaacs
ICAO	International Civil Aviation Organization
IRAC	Integrated Resilient Aircraft Control
LOC	Loss of Control
NASA	National Aeronautics and Space Administration
PDE	partial differential equations

List of Symbols

Greek Symbols

α	Angle of attack [rad]
β	Sideslip angle [rad]
γ	Flight path angle [rad]
Δ_x, Δ_z	Shift in center of gravity [m]
δ_a, δ_e, δ_f δ_r	Aileron, elevator, flap and rudder deflection [rad]
$\nabla_{\mathbf{x}}$	Gradient of value function
$\eta_{p_\bullet}, \eta_{\delta_{a_\bullet}}$	Parameters of yaw moment polynomial model with angle of attack
ρ	Air density [kg/m^2]
τ	Time instant [s]
$\Phi(\mathbf{x})$, Φ_t	Viscous approximation of value function and its time derivative
ϕ	State trajectory
ϕ, θ, ψ	Euler angles [rad]
$\partial\Omega$	Interface: Boundary of a set or a region

Roman Symbols

b	Wingspan [m]
$\bar{c}$	Mean aerodynamic chord [m]
$C_{Y_\bullet}, C_{l_\bullet}$, $C_{n_\bullet}$	Lateral aerodynamic derivatives
$C_{L_\bullet}$, $C_{D_\bullet}$, $C_{m_\bullet}$	Longitudinal aerodynamic derivatives
d_x, d_z	Perpendicular distance of lost part from new center of gravity [m]
D_t	Differential operator in time

$\mathbf{f}$	Nonlinear continuous dynamic system
g_1, g_2, g_3	Gravity components in wind axes [m/s^2]
$g(x)$	Terminal cost function
H^i, H^t	Hamiltonian for initial and terminal value problem
$\mathcal{I}$, $\mathcal{V}$	Invariance set and Viability set
$J_\bullet$	Aircraft mass moment of inertia [kg.m^2]
K, L	Set of States
l	Implicit function
$\ell_{\beta_\bullet}$, $\ell_{p_\bullet}$, $\ell_{r_\bullet}$	Parameters of roll moment polynomial model with angle of attack
m	Mass of aircraft [kg]
$m_{damaged}$	Mass of damaged aircraft [kg]
p, q, r	Body angular rates [rad/s]
$\mathcal{R}_\mathcal{F}$, $\mathcal{R}_\mathcal{B}$	Forward and backward reachable sets
r_z	Thrust moment arm in $z-$axis [m]
S	Wing area [m^2]
T	Time horizon [s], Total thrust [N]
t	Time [s]
U	Set of control inputs
$\mathbf{u}$	Control input signal
$\mathbf{u}^*$	Optimal control input signal
V_1, V_2	Value functions for viability and invariance, respectively
V	Velocity [m/s^2]
x, y, h	Flat earth east, Flat earth north and Altitude [m]
$\mathbf{x}$, $\dot{\mathbf{x}}$	State of the system and time derivative of the state
$\mathcal{Y}_{p_\bullet}$	Parameters of side force polynomial model with angle of attack

List of Figures

List of Tables

Contents

Part I

Technical Paper

Effects of Structural Failures on the Safe Flight Envelope of Aircraft

H. N. Nabi* and C. C. de Visser†

The research presented in this paper focuses on the effects of structural failures on the safe flight envelope of an aircraft. Nonlinear reachability analysis using the level set method is performed to estimate the safe flight envelope through an optimal control formulation using actual aircraft control inputs. This approach utilizes the physical model of an aircraft based upon the flight dynamics, where the aerodynamic stability and control derivatives are estimated using Digital Datcom. The database of safe flight envelopes computed offline corresponding to different structural failures at various flight conditions will allow real time flight envelope prediction and protection. This research provides an insight into the feasibility of such a database approach. Symmetrical damages to an aircraft were considered with 25%, 50%, 75% and 100% spanwise vertical tail tip loss, leading to gradual shrinkage in the safe flight envelope. Based on the estimated safe flight envelopes, a discussion on the effects of structural damages and different flight conditions on the safe flight envelope is presented.

Nomenclature

$\mathcal{B}$	Set of allowable/achievable states and input vectors
b	Wingspan [m]
$C_\bullet$	Aerodynamic derivatives
$\bar{c}$	Mean aerodynamic chord [m]
d_x, d_z	Perpendicular distance of lost part from new center of gravity [m]
$\mathbf{f}$	Nonlinear continuous dynamic system
g_1, g_2, g_3	Gravity components in wind axes [m/s^2]
H	Hamiltonian
J	Cost function
$J_\bullet$	Aircraft mass moment of inertia [kg.m^2]
K	Set of states
L	Set of states
l	Implicit function
$\ell_{\beta_\bullet}$, $\ell_{r_\bullet}$	Parameters of roll moment polynomial model with angle of attack
m	Mass of aircraft [kg]
$m_{damaged}$	Mass of damaged aircraft [kg]
$\mathbf{p}$	Co-state vector
p, q, r	Body angular rates [rad/s]
r_z	Thrust moment arm in $z-$axis [m]
S	Wing Area [m^2]
T	Time horizon [s], Total Thrust [N]
t	Time [s]
$t_{\mathcal{F}}$, $t_{\mathcal{B}}$	Computational time for forward and backward reachable sets [s]
$\mathbf{U}$	Set of control inputs

*MSc. Student, Department of Control and Simulation, Delft University of Technology, Kluyverweg 1 2629 HS Delft, The Netherlands.

†Assistant Professor, Department of Control and Simulation, Delft University of Technology, Kluyverweg 1 2629 HS Delft, The Netherlands.

$\mathbf{u}$	Control input signal
V	Velocity [m/s]
$\mathcal{V}$, $\mathcal{I}$, $\mathcal{R}$	Viability, Invariance and Reachability set
V_1	Value function for viability
V_2	Value function for invariance
$W_\bullet$	Weights in cost function
$\mathcal{Y}_{p_\bullet}$	Parameters of side force polynomial model with angle of attack
$\mathbf{x}$, $\dot{\mathbf{x}}$	State of the system and time derivative of the state
x, y, h	Flat earth east, Flat earth north and Altitude [m]
α	Angle of attack [rad]
β	Sideslip Angle [rad]
γ	Flight path angle [rad]
Δ_x, Δ_z	Shift in center of gravity [m]
δ_a, δ_e, δ_f δ_r	Aileron, Elevator, Flap and Rudder deflection [rad]
$\eta_{p_\bullet}$, $\eta_{\delta_{a_\bullet}}$	Parameters of yaw moment polynomial model with angle of attack
ρ	Air density [kg/m^2]
τ	Time instant [s]
ϕ	State trajectory
ϕ, θ, ψ	Euler angles [rad]

Subscripts

$\mathcal{B}$, $\mathcal{F}$	Backward and Forward
HT, VT, F	Horizontal tail, Vertical tail and Dorsal fin

Superscripts

c	Set compliment

I. Introduction

Air travel is one of the safest modes of transport. This has been possible due to a continuous focus on aviation safety over the years. A number of studies have been conducted to investigate the causes of in-flight failures and to recommend the necessary steps to prevent such failures in the future. One such study by CAST/ICAO shows that the Loss of Control (LOC) in flight is the primary cause of fatal accidents in civil aviation. The study presents a statistical analysis of aircraft accidents during the period of 2002 till 2011 and it is indicated that the LOC comprises of as much as 23% of all catastrophic aircraft accidents.[1] LOC entails that the aircraft has left the safe flight envelope, which is the set of safe flight conditions. With regards to flight performance, structural damages to the aircraft or control actuator failures deteriorate the flying qualities, hence, require immediate attention to maintain the integrity of an aircraft and to safely land the aircraft.[2] Because of the degraded flying qualities due to damage, the safe flight envelope may *shrink* and the aircraft may find itself outside of this changed safe flight envelope, which leads to LOC. Figure 1 shows such a scenario. Although the system dynamics may change completely as a result of a damage, LOC related accidents can still be prevented using unconventional control strategies.

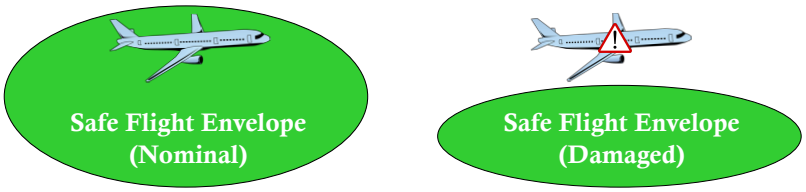

(a) Nominal Aircraft (b) Damaged Aircraft

Figure 1. Loss of Control due to Damage

In order to prevent LOC, it is very important to have knowledge about the restricted safe flight envelope of an impaired aircraft,[3–5] so that it can be ensured that the aircraft does not leave the safe flight envelope. This information can also be used to improve pilot's overall situation awareness significantly.[4,5]

The flight envelope has been estimated in the literature by means of various methods. The estimation

methods include wind tunnel testing, flight experiments and the model based computation of achievable trim points[6,7] or using a vortex lattice algorithm coupled with an extended kalman filter to estimate the performance flight envelope.[8] A more extensive and rigorous method is to estimate the safe flight envelope by considering it to be a non-linear reachability problem and to obtain the solution by numerically solving the Hamilton Jacobi Bellman (HJB) partial differential equations or Hamilton Jacobi Isaacs (HJI) equations when the presence of disturbances are considered in the analysis. Reachability analysis allows a very detailed and accurate estimation of the safe flight envelope, however, the major challenge associated with such an analysis is the *"curse of dimensionality"*.[9] Therefore, it limits the application of available numerical tools for online safe flight envelope estimation to relatively low dimensional problems. To the best of our knowledge, the maximum dimension of the safe flight envelope that has been estimated offline using the reachability analysis is four.[10,11]

In order to tackle the limitation on online safe flight envelope estimation, a database approach towards flight envelope prediction and protection was firstly introduced by Tang et al.,[12] however, the study conducted in this research was only limited to actuator failure scenarios and did not include actual control inputs, rather *"virtual inputs"* for the reachability analysis. The same concept has been recently reintroduced[13,14] and extends the implementation of the database approach to structural damages. The basic principle of the database approach, is that instead of trying to solve the HJI/HJB equations in real time, a database of safe flight envelopes corresponding to the most often occurring failures is created offline. This offline database is then carried on-board of the aircraft, and when a failure occurs, the database is accessed to obtain the stored safe flight envelopes that are closest to the actual failure. These candidate envelopes are interpolated, such that they resemble the actual failure case. The interpolated safe flight envelope is then used by the fault tolerant flight control system to prevent the aircraft from leaving the safe flight envelope, thereby preventing loss of control. Moreover, this information is also displayed to the pilot in order to improve the overall situation awareness. Figure 2 shows an overview of the database approach to flight envelope prediction and protection.

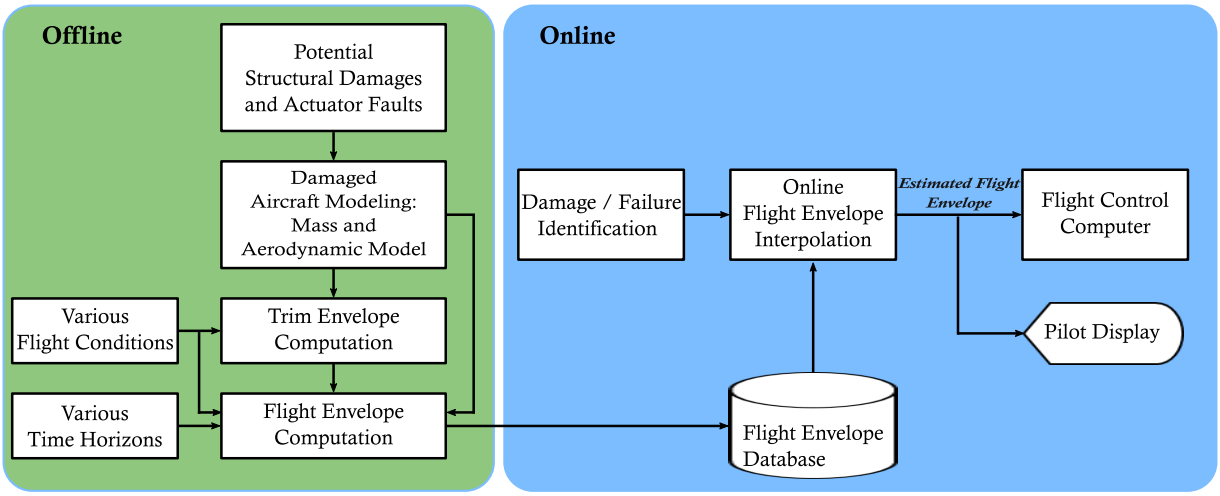

Figure 2. The Database Approach

Focus of the current paper is on the offline part of the database approach, in order to investigate the feasibility of this novel method. The main objective is to construct a database of safe flight envelopes corresponding to tip loss (in percentage of span) of vertical tail at various flight conditions. In particular, the study aims to show how structural failures affect the safe flight envelope of an aircraft and how these effects can be grouped into categories. This information is of extreme significance for the novel database approach to the real time flight envelope prediction and protection.

The paper is arranged into sections as follows: Section II presents a brief introduction of the topics related to the safe flight envelope estimation and the reachability set theory. Curse of dimensionality and the possible solutions to the problem are discussed in section III. An aerodynamic and a mass model of the damaged aircraft is presented in section IV. Sections V and VI present the trim and the safe flight envelopes for the longitudinal and the lateral motion of the aircraft respectively. Lastly, a brief conclusion is presented in section VII.

II. Reachability Set Theory and Safe Flight Envelope

The standard definition of the flight envelope refers to a region of airspeed and altitude, where an aircraft is required to operate or a constrained area in the velocity versus load factor graph. These definitions can be found in any textbook on aircraft performance.[15,16] However, for the purpose of avoiding LOC, we are interested in the safe flight envelope, which is formally defined as:[17]

The set of aircraft's state space for which the aircraft can be safely controlled and loss-of-control can easily be avoided.

This set is also referred to as the dynamic flight envelope[17] or the immediate flight envelope.[12]

II.A. Reachability Set Theory

The reachability set theory is widely used in the safety analysis. It studies the behavior of set of trajectories that emerge from a dynamic system. In particular, whether these trajectories can reach from one point to another in a given time.

Consider a continuous time system $\dot{\mathbf{x}} = \mathbf{f}(\mathbf{x}, \mathbf{u}, t)$, a time horizon $T \geq 0$, set of control inputs $\mathbf{u} \in U$ and a set of states K. There are three main sets that can be formulated associated with the set K and the trajectories that lead to K over a time horizon T.[18]

Viability $\mathcal{V}(t, K)$: Set of all the states $\mathbf{x}(\cdot)$ for which there exist at least one input $\mathbf{u}(\cdot) \in U_{[0,T]}$ such that $\mathbf{x}(t) \in K$ for all $t \in [0, T]$.

Invariance $\mathcal{I}(t, K)$: Set of all the states $\mathbf{x}(\cdot)$ for which there exist all the inputs $\mathbf{u}(\cdot) \in U_{[0,T]}$ such that $\mathbf{x}(t) \in K$ for all $t \in [0, T]$.

Reachability $\mathcal{R}(t, K)$: Set of all the states $\mathbf{x}(\cdot)$ for which there exist at least one input $\mathbf{u}(\cdot) \in U_{[0,T]}$ and $t \in [0, T]$ such that $\mathbf{x}(t) \in K$.

By comparing the above sets, it can be stated that:

$$\mathcal{I}(t, K) \subset \mathcal{V}(t, K) \subset \mathcal{R}(t, K) \tag{1}$$

Moreover, the principle of duality relates the reachability and the invariant set as follows:

$$\mathcal{R}(t, K) = (\mathcal{I}(t, K^c))^c \tag{2}$$

Figure 3 shows an illustration of these three sets. The smallest of these sets, as stated in Eq. 1, is the invariant set. It is the set of states where all the inputs lead to trajectories that remain inside the trim set K throughout the time horizon T. Next is the viability set, which is the largest subset of the trim set K. It can be seen that there are trajectories extending outside the trim set K, however, there is at least one input that keeps the trajectory inside the trim set over the time horizon T. Lastly, the reachability set consists of all the states within and outside the trim set K for which at least one input $\mathbf{u}(\cdot)$ can bring the trajectory to the target set K within a time $t \in [0, T]$.

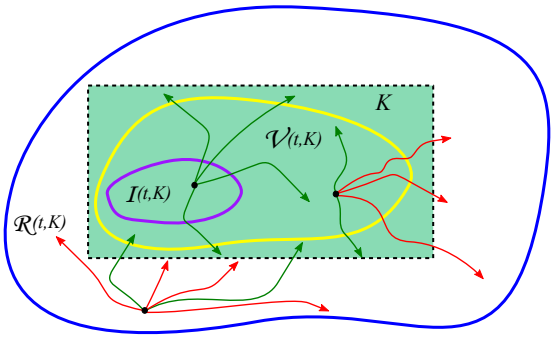

Figure 3. Viability (Yellow), Invariance (Magenta) and (backward) Reachability Set (Blue), Green: Successful trajectories; Red: Unsuccessful trajectories

The system $\dot{\mathbf{x}} = \mathbf{f}(\mathbf{x}, \mathbf{u}, t)$ can be evolved forward and backwards in time, which can give us two further types of reachability sets; forward and backward reachable sets:

Forward Reachable Set $\mathcal{R}_{\mathcal{F}}(t,K)$: Set of all the states $\mathbf{x}(\cdot)$ for which a control input $\mathbf{u}(\cdot) \in U_{[0,T]}$ exists at time $t \in [0,T]$, such that this set can be approached from at least one point in the trim envelope K.

Backward Reachable Set $\mathcal{R}_{\mathcal{B}}(t,K)$: Set of all the states $\mathbf{x}(\cdot)$ for which a control input $\mathbf{u}(\cdot) \in U_{[0,T]}$ exists at time $t \in [0,T]$, such that at least one state in the trim envelope K can be reached.

The *viability* and the *invariant* set can be linked to SUPMIN and INFMIN optimal control problems respectively.[18] Suppose that the open set K is associated with the zero level set of a function $l : \mathbb{R}^n \to \mathbb{R}$ by $K = \{\mathbf{x} \in \mathbb{R}^n \,|\, l(\mathbf{x}) > 0\}$, then the viability set can be given as:

$$\mathcal{V}(t,K) = \left\{ \mathbf{x} \in \mathbb{R}^n | V_1(\mathbf{x},t) = \sup_{\mathbf{u}(\cdot)\in U_{[t,T]}} \min_{\tau\in[t,T]} l\left(\phi\left(\tau,t,\mathbf{x},u(\cdot)\right)\right) > 0 \right\} \tag{3}$$

In the above equation $\phi(\tau,t,\mathbf{x},u(\cdot))$ is the state trajectory. Similarly, assume a closed set L that is associated with the level set of a continuous function $l : \mathbb{R}^n \to \mathbb{R}$ by $L = \{\mathbf{x} \in \mathbb{R}^n \,|\, l(\mathbf{x}) \geq 0\}$, then the invariant set can be expressed as:

$$\mathcal{I}(t,K) = \left\{ \mathbf{x} \in \mathbb{R}^n | V_2(\mathbf{x},t) = \inf_{\mathbf{u}(\cdot)\in U_{[t,T]}} \min_{\tau\in[t,T]} l\left(\phi\left(\tau,t,\mathbf{x},u(\cdot)\right)\right) \geq 0 \right\} \tag{4}$$

It is suggested by Lygeros,[18] that the characterization of value functions V_1 and V_2, given in Eqs. 3 and 4 respectively, can be represented as viscosity solutions to Hamilton-Jacobi partial differential equations. Hence the viability set can be written in the form of HJB PDE as:

$$\frac{\partial V_1}{\partial t}(\mathbf{x},t) + \min_{\tau\in[t,T]} \left\{ 0, \sup_{\mathbf{u}(\cdot)\in \mathrm{U}_{[t,T]}} \frac{\partial V_1}{\partial \mathbf{x}}(\mathbf{x},t)\, \mathbf{f}(\mathbf{x},\mathbf{u},t) \right\} = 0 \tag{5}$$

And the invariant set is written in the form of HJB PDE as:

$$\frac{\partial V_2}{\partial t}(\mathbf{x},t) + \min_{\tau\in[t,T]} \left\{ 0, \inf_{\mathbf{u}(\cdot)\in \mathrm{U}_{[t,T]}} \frac{\partial V_2}{\partial \mathbf{x}}(\mathbf{x},t)\, \mathbf{f}(\mathbf{x},\mathbf{u},t) \right\} = 0 \tag{6}$$

The HJ PDE given by Eqs. 5 and 6 can be solved either as an initial value problem or a terminal value problem in order to compute a forward or a backward set respectively. Moreover, the principle of duality as defined by Eq. 2, is used to obtain the reachability set. Eqs. 5 and 6 are solved numerically using the level set toolbox developed in MATLAB® at Stanford University,[19,20] using the algorithm presented by Osher and Fedkiw.[21]

II.B. Safe Flight Envelope as a Reachable Set

Safe flight envelope estimation as a reachability set problem has been researched in the recent past,[11,17,18,22] the same with uncertainty quantification and robustness in the estimated values of aerodynamic derivatives is also discussed in detail.[23,24] The idea is to observe the dynamic behavior of the trim states as they evolve over a certain time horizon T i.e., reachability from the trim envelope (set of trim states). The trim envelope, which is the set of stable and controllable states, is considered as a-priori safe set. In terms of reachability set, the *safe flight envelope* is defined as the set of states, that lie in the intersection of forward and backward reachable sets. The forward reachable set refers to the set of states to which an aircraft can easily maneuver from the stable trim set. On the other hand, the backward reachable set (or the survivable envelope[24]) refers to the set of states from where an aircraft can recover back to the stable trim set. Hence, the safe set is the intersection between the aircraft's capability to maneuver from the trim set (forward reachable set) and the survivable capacity of an aircraft (backward reachable set). This is illustrated in Figure 4.

Note, that it is very important to define an accurate trim set in order to obtain a correct reachability set. Any untrimmed state which is part of the initial set will lead to an inaccurate safe flight envelope. Computation of the trim states have been discussed extensively in the existing literature. A common approach to compute the trim set is to minimize a cost function using a numerical optimization routine.[25,26] Other approaches to obtain the trim set include the interval analysis[27] and bifurcation and continuation methods.[28]

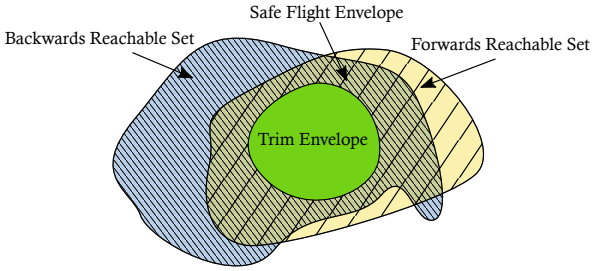

Figure 4. Safe Flight Envelope[17]

III. Curse of Dimensionality

Estimating the safe flight envelope as a reachability set using the level set method is computationally expensive; the time and the memory required grow significantly with an increase in the problem's dimension. The computational complexity of the level set method is of the order $\mathcal{O}\left(N^{n+1}\right)$, with N being the number of computational grid points and n the dimension of the problem.[29] It has been suggested by Kitsios and Lygeros[9] that the *"curse of dimensionality"* in the reachability analysis can be solved by exploiting the structure of the system dynamics using the principle of time scale separation and solving the reachability problem in a sequential manner; first for the faster dynamics and then for the slower dynamics.

Figure 5 shows the structure of time scale separation implemented for reachability computation by Kitsios and Lygeros.[9] First, the range of pseudo-controls (V, γ) is computed by defining the reachability problem for faster dynamics. In the next step, the viability set for the states with slower dynamics (x, y, h, ψ) has been estimated using the pseudo-controls (V, γ) and the actual optimal inputs (C_L, ϕ). This allows solving the higher dimensional reachability problem in two steps of lower dimensional reachability problems (two and four respectively). However, although the dynamics has been split into faster and slower dynamics, these six states belong to the low bandwidth dynamics and are slower than the states belonging to high bandwidth (faster) dynamics, such as body angular rates and aerodynamic angles. The states belonging to fast dynamics will be of interest in case of a structural failure to the aircraft. Moreover, the reachability computation performed by Kitsios and Lygeros do not consider actual control inputs to the system rather *"virtual inputs"* in the form of lift coefficient C_L and roll angle ϕ.

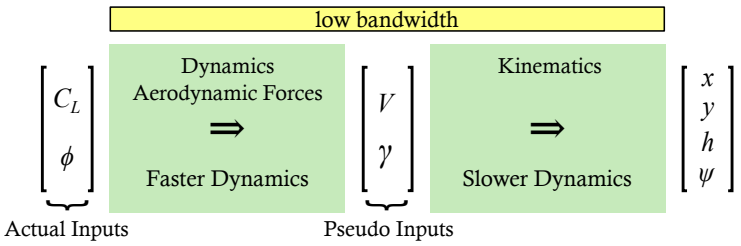

Figure 5. Time Scale Separation implemented by Kitsios and Lygeros[9]

Lombaerts et al.[24] has suggested a structure that incorporates faster dynamics and include actual aircraft control inputs for the reachability computation. This decomposition of aircraft dynamics based on the principle of time scale separation is presented in Figure 6. However, the sequence of reachability computation for faster dynamics suggested here is not feasible when only considering the control surface deflections as inputs for the reachability analysis. Consider the nine-dimensional equations of motion of an aircraft.[30] Firstly, the moment equations of motion in the body-fixed reference frame are given by:

$$\begin{cases} \dot{p} = (c_1 r + c_2 p)\, q + c_3 \frac{1}{2}\rho V^2 S b C_l\left(\alpha, \beta, p, r, \delta_a, \delta_r\right) + c_4 \frac{1}{2}\rho V^2 S b C_n\left(\alpha, \beta, p, r, \delta_a, \delta_r\right) \\ \dot{q} = c_5 p r - c_6\left(p^2 - r^2\right) + c_7 \frac{1}{2}\rho V^2 S \bar{c} C_m\left(\alpha, q, \delta_e\right) \\ \dot{r} = (c_8 p - c_2 r)\, q + c_4 \frac{1}{2}\rho V^2 S b C_l\left(\alpha, \beta, p, r, \delta_a, \delta_r\right) + c_9 \frac{1}{2}\rho V^2 S b C_n\left(\alpha, \beta, p, r, \delta_a, \delta_r\right) \end{cases} \tag{7}$$

where the moments of inertia are defined as, with $\Gamma = J_{xx} J_{zz} - J_{zx}^2$:

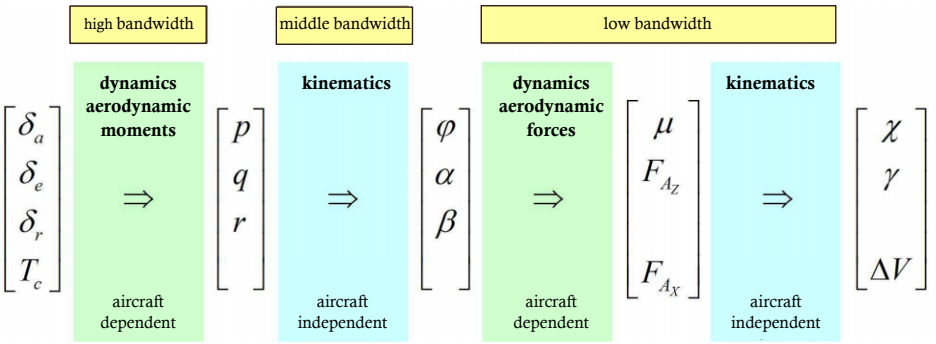

Figure 6. Time Scale Separation of Aircraft Dynamics[24]

$$\Gamma c_1 = (J_{yy} - J_{zz})\, J_{zz} - J_{zx}^2 \qquad \Gamma c_4 = J_{zx} \qquad c_7 = \frac{1}{J_{yy}}$$

$$\Gamma c_2 = (J_{xx} - J_{yy} + J_{zz})\, J_{zx} \qquad c_5 = \frac{J_{zz} - J_{xx}}{J_{yy}} \qquad \Gamma c_8 = (J_{xx} - J_{yy})\, J_{xx} + J_{zx}^2$$

$$\Gamma c_3 = J_{zz} \qquad c_6 = \frac{J_{zx}}{J_{yy}} \qquad \Gamma c_9 = J_{xx}$$

Secondly, the force equations of motion in the wind-axes reference frame are:

$$\begin{cases} \dot{V} = \dfrac{1}{m}\left(T\cos\alpha\cos\beta - \frac{1}{2}\rho V^2 S C_D(\alpha) + mg_1\right) \\ \dot{\beta} = p\sin\alpha - r\cos\alpha + \dfrac{1}{mV}\left[-T\cos\alpha\sin\beta + \frac{1}{2}\rho V^2 S C_Y(\alpha,\beta,p,\delta_r) + mg_2\right] \\ \dot{\alpha} = q - p\cos\alpha\tan\beta - r\sin\alpha\tan\beta + \dfrac{1}{mV\cos\beta}\left[-T\sin\alpha - \frac{1}{2}\rho V^2 S C_L(\alpha,q,\delta_f) + mg_3\right] \end{cases} \tag{8}$$

where the components of the gravity vector in wind-axes are given by:

$$\begin{aligned} g_1 &= g\,(-\cos\alpha\cos\beta\sin\theta + \sin\beta\sin\phi\cos\theta + \sin\alpha\cos\beta\cos\phi\cos\theta) \\ g_2 &= g\,(\cos\alpha\sin\beta\sin\theta + \cos\beta\sin\phi\cos\theta - \sin\alpha\sin\beta\cos\phi\cos\theta) \\ g_3 &= g\,(\sin\alpha\sin\theta + \cos\alpha\cos\phi\cos\theta) \end{aligned}$$

And lastly, the kinematic equations are written as:

$$\begin{cases} \dot{\phi} = p + \tan\theta\,(q\sin\phi + r\cos\phi) \\ \dot{\theta} = q\cos\phi - r\sin\phi \\ \dot{\psi} = q\frac{\sin\phi}{\cos\theta} + r\frac{\cos\phi}{\cos\theta} \end{cases} \tag{9}$$

From Eqs. 7 and 8, it can be seen that the p, q, r and V, β, α are dependent upon each other. Therefore, the safe flight envelope for angular rates (p, q, r) cannot directly be obtained using the reachability computation without the information about the bounds of velocity V, sideslip angle β and angle of attack α; yet the safe flight envelope for V, β and α is computed at the later stage according to this structure, see Figure 6. Similarly, in order to obtain the safe flight envelope for V, β and α, we need the information about the safe flight envelope for Euler angles (ϕ, θ, ψ) and in order to compute the safe flight envelope for Euler angles, we again require the information of angular rates, see Eq. 9. It can be concluded, that although the principle of time scale separation is useful for the slow dynamics as suggested by Kitsios and Lygeros,[9] it is not feasible and possible to use the same principle of time scale separation for the fast dynamics. All in all, a nine-dimensional reachability problem has to be solved, which is not feasible with the current computational potential.

Estimation of the safe flight envelope in a reachability framework using the actual aircraft control inputs (stabilizer deflection and engine thrust) has only been discussed once.[11,17] Apart from that, in the literature hitherto,[5,9,12,18,23,24] reachability computation has only been performed for the slower dynamics and

therefore, the angle of attack and the sideslip angle etc. have been used as the "*virtual inputs*". However, the changes in the safe flight envelope of these virtual inputs due to a structural damage or a system failure is not considered. In contrast, in the current paper the safe flight envelope for the states with fast dynamics has been estimated using the actual control surface inputs.

For the current research, the problem of "curse of dimensionality" is addressed by decoupling the dynamics into longitudinal and lateral dynamics. Such a generalized structure for the safe flight envelope estimation is shown in Figure 7. The longitudinal dynamics is further reduced to a three dimensional problem by considering velocity V to be constant and varying thrust T to maintain the velocity. Also, the lateral dynamics is reduced to a two dimensional problem by considering $p = \phi = 0$ and varying aileron deflection δ_a to keep the wings level.

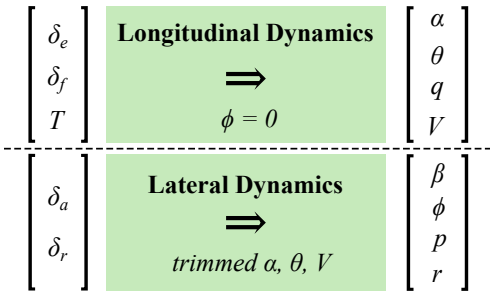

Figure 7. Safe Flight Envelope Estimation using Decoupled Dynamics

It should be noted, that the decomposition of aircraft dynamics into longitudinal and lateral dynamics for the reachability analysis will not be valid for the asymmetric damages due to inertial couplings. Therefore, for the current research only symmetrical damages (spanwise damage to the vertical tail) are considered. The spanwise damage to the vertical tail along with different flight conditions, will give a significant insight into the feasibility of the database approach.

IV. Modeling of the Damaged Aircraft

Solving the reachability problem using the level set method rely on the physical model as indicated by the term $\mathbf{f}(\mathbf{x}, \mathbf{u}, t)$ in Eqs. 5 and 6. Hence, in order to estimate the safe flight envelope, it is essential to have a dynamic model of an aircraft. One of the key parts of such a dynamic model is the aerodynamic model. The aerodynamic models can either be simple polynomial models or more complex multivariate spline models.[31] In case of a structural damage to an aircraft the aerodynamic model parameters, in addition to mass and inertial properties of the aircraft, will change. Furthermore, changes in the model structure may also arise due to inertial couplings. The additional parameters that may appear in the model structure of an asymmetrically damaged aircraft can be estimated either by wind tunnel testing or by a Computational Fluid Dynamics (CFD) analysis. A detailed wind tunnel research was conducted at the NASA Langley Research Center in order to study the effects on the aerodynamic model parameters (such as pitching moment coefficient C_m, rolling moment coefficient C_l etc.) of different damage case scenarios to a conventional transport aircraft.[32] Moreover, Bacon and Gregory[33] from NASA Langley Research Center have presented a set of flight dynamics equations of motion for an asymmetrically damaged aircraft. In the current research, however, only symmetrical damages are investigated i.e., spanwise damage to the vertical tail, as mentioned in the previous section. Model parameters for the nominal and the damaged aircraft are estimated using Digital Datcom.[34] Cessna Citation II laboratory aircraft (PH-LAB), Figure 8, is used as a reference aircraft for the damage modeling.

IV.A. Assumptions

- The mass of the horizontal tail and vertical tail is assumed to be 2.5% of the total empty mass of the aircraft and the mass of the dorsal fin is assumed to be 0.5% of the total empty mass of the aircraft.
- x% damage to the vertical tail entails x% loss in the span of the vertical tail and x% loss in the mass of the vertical tail.

Figure 8. Cessna Citation II Laboratory Aircraft

- In case of 100% vertical tail loss, it is assumed that the horizontal tail and the dorsal fin are also lost.
- Digital Datcom[34] does not provide the rudder control derivatives and hence actual values for the Cessna Citation II have been used. For the damaged vertical tail, it is assumed that the degradation in control effectiveness of rudder is linear with the damage. That is, $x\%$ loss of vertical tail will lead to $x\%$ degradation in $C_{n_{\delta_r}}$, $C_{l_{\delta_r}}$ and $C_{Y_{\delta_r}}$.

IV.B. Effects of Damage on the Geometry and Mass Properties of the Aircraft

IV.B.1. Change in Vertical Tail Chord Length

It is assumed that the increase in chord length from tip to root is linear, see Figure 9. Therefore the tip chord of damaged vertical tail is given by:

$$c_{tip_{damaged}} = \left(\frac{c_{tip_{original}} - c_{root_{original}}}{b_{original}} \right) b_{damaged} + c_{root_{original}} \tag{10}$$

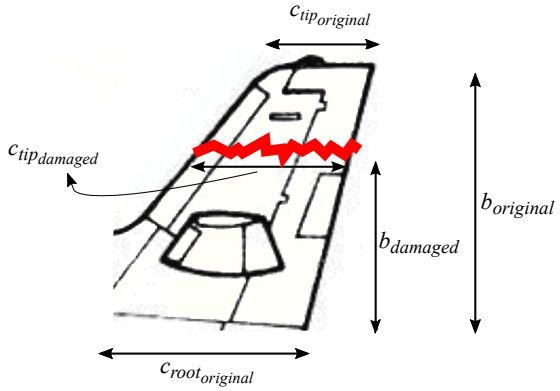

Figure 9. Vertical Tail Damage

IV.B.2. Change in the Mass of the Aircraft

From the second assumption, mentioned in the previous section, the mass of the damaged aircraft is given as follows:

$$m_{damaged} = m_{original} - x\% \cdot m_{VT} \tag{11}$$

In case of 100% vertical tail loss, the mass of the damaged aircraft is then computed as:

$$m_{damaged} = m_{original} - m_{VT} - m_{HT} - m_F \tag{12}$$

where m_{VT} is the vertical tail mass, m_{HT} is the horizontal tail mass and m_F is the mass of the dorsal fin.

IV.B.3. Change in the Center of Gravity Location

Due to the symmetrical nature of the damage, the movement of center of gravity in y-body axis is neglected. Furthermore, it is assumed that the change in center of gravity location is proportional to the loss in mass i.e.,

$$\begin{aligned} c.g._{damaged} &= \left(\frac{m_{damaged}}{m_{original}}\right) c.g._{original} \qquad \text{(c.g. moving towards origin)} \\ c.g._{damaged} &= \left(\frac{m_{original}}{m_{damaged}}\right) c.g._{original} \qquad \text{(c.g. moving away from origin)} \end{aligned} \tag{13}$$

IV.B.4. Change in the Mass Moments of Inertia

Changes in the moments of inertia due to damage are caused by two main factors; 1) change in the position of the center of gravity and 2) change in the mass of the aircraft. Therefore, both of these factors should be taken into account for estimating the modified moment of inertia.

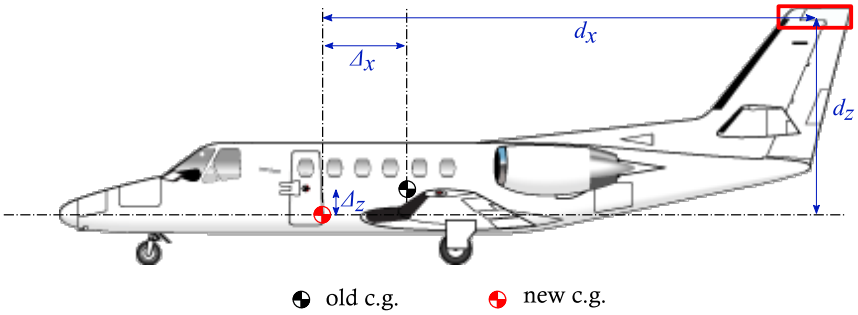

Figure 10. Center of Gravity shift due to Tail Damage

Referring to Figure 10, the moment of inertia of the damaged aircraft is estimated by the following formula:

$$\begin{aligned} &J_{i_{damaged}} = J_{i_{original}} + m_{damaged}{\Delta_j}^2 - (J_{i_{LostPart}} + m_{LostPart}{d_j}^2) \\ &\text{where} \quad i = xx, yy, zz \quad \text{and} \quad j = z, z, x \end{aligned} \tag{14}$$

In the above equation $m_{damaged}{\Delta_j}^2$ is the correction for the change in the center of gravity location using the parallel axis theorem. The moment of inertia for the lost part is then subtracted from the overall inertia. It is assumed that the lost part is a rectangular prism, with thickness equal to the maximum thickness of the airfoil.[35]

The physical parameters of Cessna Citation II are shown in Table 1 for the nominal and the damaged aircraft, as estimated by methods described above. The mass and the inertia is decreasing with the damage and the tip chord of the vertical tail is increasing, as expected. Moreover, the damage causes the center of gravity to move towards the nose horizontally and away from aircraft's centerline vertically.

IV.C. Effects of Damage on the Aerodynamic Parameters

Aerodynamic effects of the structural damages were estimated using USAF Digital Datcom.[34] Digital Datcom estimates the derivatives of symmetrical aircraft using the methods contained in the USAF Stability

Table 1. Physical Parameters of Cessna Citation II

Vertical Tail Tip Loss [%]	**0**	**25**	**50**	**75**	**100**
Mass of Aircraft [kg]	5,500	5,477.2	5,454.3	5431.5	5,299
Tip chord of VT [m]	1.11	1.465	1.82	2.175	–
J_{xx} [kg.m^2]	26,032	25,779	25,622	25,540	25,280
J_{yy} [kg.m^2]	36,388	36,131	35,966	35,869	35,632
J_{zz} [kg.m^2]	59,818	59,131	58,435	57,726	53,556
J_{zx} [kg.m^2]	2,717.8	2,301.5	1,971.4	2,058.5	790.9
$x_{c.g.}$ (origin at nose) [m]	6.78	6.7518	6.7237	6.6955	6.5322
$z_{c.g.}$ (origin at nose) [m]	-0.05	-0.0502	-0.0504	-0.0506	-0.0519
Thrust moment arm r_z [m]	0.6784	0.6786	0.6788	0.6790	0.6803
S [m^2]	30				
$\bar{c}$ [m]	2.06				
b [m]	15.9				

and Control Datcom (Data Compendium).[36] Digital Datcom allows the estimation of static stability, control device and dynamic derivative characteristics of various symmetrical configurations at different flight conditions.

Based on the aerodynamic parameters that can be estimated using Digital Datcom, the following aerodynamic polynomial model is constructed:

$$Longitudinal \begin{cases} C_L = C_{L_0} + C_{L_\alpha}\alpha + C_{L_q}\frac{q\bar{c}}{2V} + C_{L_{\delta_f}}\delta_f \\ C_D = C_{D_0} + C_{D_\alpha}\alpha + C_{D_{\alpha^2}}\alpha^2 \\ C_m = C_{m_0} + C_{m_\alpha}\alpha + C_{m_q}\frac{q\bar{c}}{2V} + C_{m_{\delta_e}}\delta_e \end{cases} \tag{15}$$

$$Lateral \begin{cases} C_Y = C_{Y_0} + C_{Y_\beta}\beta + (\mathcal{Y}_{p_0} + \mathcal{Y}_{p_\alpha}\alpha)\frac{pb}{2V} + C_{Y_{\delta_r}}\delta_r \\ C_l = C_{l_0} + (\ell_{\beta_0} + \ell_{\beta_\alpha}\alpha)\beta + C_{l_p}\frac{pb}{2V} + (\ell_{r_0} + \ell_{r_\alpha}\alpha)\frac{rb}{2V} + C_{l_{\delta_a}}\delta_a + C_{l_{\delta_r}}\delta_r \\ C_n = C_{n_0} + C_{n_\beta}\beta + (\eta_{p_0} + \eta_{p_\alpha}\alpha)\frac{pb}{2V} + C_{n_r}\frac{rb}{2V} + (\eta_{\delta_{a0}} + \eta_{\delta_{a\alpha}}\alpha)\delta_a + C_{n_{\delta_r}}\delta_r \end{cases} \tag{16}$$

The last terms in Eq. 16 are the rudder control derivatives and are estimated by the method described in the final assumption. Furthermore, few of the lateral stability derivatives estimated by Digital Datcom vary with the angle of attack. Additional parameters of these lateral stability derivatives for a linear polynomial model in angle of attack are defined as follows:

$$\begin{aligned} C_{l_\beta} &= \ell_{\beta_0} + \ell_{\beta_\alpha}\alpha \\ C_{l_r} &= \ell_{r_0} + \ell_{r_\alpha}\alpha \\ C_{n_p} &= \eta_{p_0} + \eta_{p_\alpha}\alpha \\ C_{n_{\delta_a}} &= \eta_{\delta_{a_0}} + \eta_{\delta_{a_\alpha}}\alpha \\ C_{Y_p} &= \mathcal{Y}_{p_0} + \mathcal{Y}_{p_\alpha}\alpha \end{aligned} \tag{17}$$

The flight conditions for which the aerodynamic parameters are estimated, are summarized in Table 2. Figure 11 shows the geometry of Cessna Citation II as approximated by Digital Datcom.

Table 2. Flight Conditions for Digital Datcom Analysis

Altitude [m]	[0 5,000 10,000]
Mach [–]	[0.2 0.3 0.4]
Angle of Attack [deg.]	[-14 : 14]

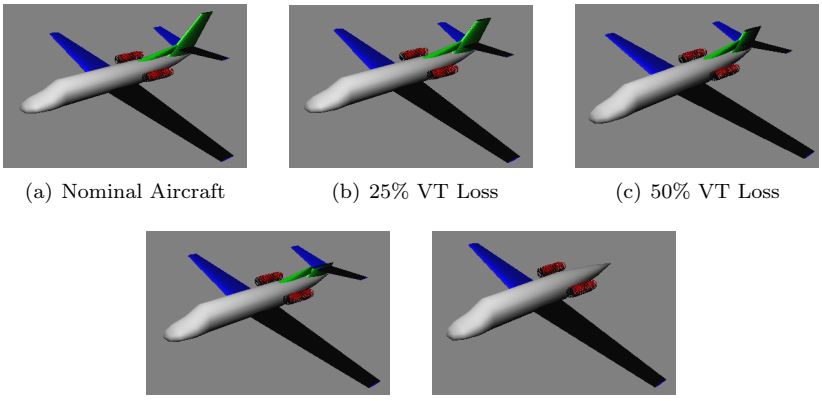

(a) Nominal Aircraft (b) 25% VT Loss (c) 50% VT Loss

(d) 75% VT Loss (e) 100% Tail Loss

Figure 11. Datcom Output of Cessna Citation II

The static and the dynamic stability derivatives that are affected most by the vertical tail damage are shown in Figure 12. The first row of plots shows the variation of the side force coefficient and the yawing moment coefficient with the sideslip angle. With the loss in the vertical tail, the sideslip generates less side force compared to the force generated for a nominal aircraft. Moreover, with 50% loss in the vertical tail, the aircraft is already directionally unstable, which can be seen by the negative slope C_{n_β}. From the third plot, it can be seen that the yaw damping characteristics exhibit a similar degrading effect throughout the angle of attack range. Lastly, it is very interesting to look at the C_{m_α} variation with the angle of attack. There is an improvement in the static longitudinal stability with the loss of vertical tail, but as soon as the complete tail is lost, the aircraft becomes longitudinally unstable. The improvement in the static longitudinal stability with spanwise loss in the vertical tail is due to the fact that the center of gravity is moving forward and hence making the aircraft more longitudinally stable; whereas, longitudinal instability with complete tail lost is rather intuitive and self-explanatory.

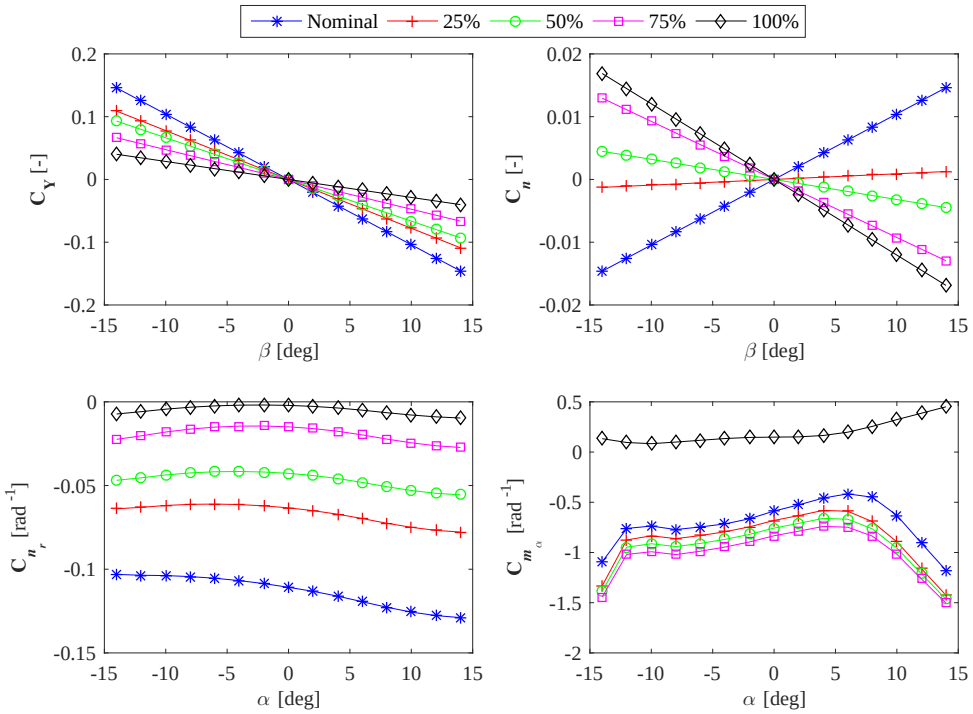

Figure 12. Effects of Vertical Tail Damage (Tip Loss in Percentage of Span) on Stability Derivatives at Mach 0.4, Sea Level

V. Longitudinal Envelope

Longitudinal motion is the motion in the aircraft's plane of symmetry ($x-z$ plane) and is characterized by the state variables: velocity V, angle of attack α, pitch rate q and pitch angle θ. Since the lateral motion is not involved, all the state variables associated with the lateral motion are set to zero i.e.,

$$\beta = \phi = p = r = 0$$

Applying these conditions to the equations of motion described by Eqs. 7, 8 and 9 will result in the longitudinal equations of motion:

$$\begin{cases} \dot{V} = \dfrac{1}{m}\left(T\cos\alpha - \frac{1}{2}\rho V^2 S C_D(\alpha) - mg\sin(\theta-\alpha)\right) \\ \dot{\alpha} = q + \dfrac{1}{mV}\left(-T\sin\alpha - \frac{1}{2}\rho V^2 S C_L(\alpha, q, \delta_f) + mg\cos(\theta-\alpha)\right) \\ \dot{q} = \dfrac{1}{J_{yy}}\left(\frac{1}{2}\rho V^2 S\bar{c} C_m(\alpha, q, \delta_e) - Tr_z\right) \\ \dot{\theta} = q \end{cases} \tag{18}$$

The additional term Tr_z in the moment equation is the pitching moment generated by Thrust. The model structure of aerodynamic coefficients (C_D, C_L, C_m) is given by Eq. 15.

V.A. Longitudinal Trim Envelope

As described earlier, in order to estimate an accurate safe flight envelope, it is absolutely essential to determine a correct trim envelope. The trim envelope is the set of stable and equilibrium states for which the state derivatives are equal to zero i.e., $\{\mathbf{x}|\mathbf{f}(\mathbf{x},\mathbf{u},t)=0, (\mathbf{x},\mathbf{u})\in\mathcal{B}\}$, where $\mathcal{B}$ represents the bound on the control inputs and the allowable states where the model is valid.

The trim envelope is commonly estimated by minimizing a cost function for some fixed states. The cost function for the longitudinal motion that is minimized using the `fminsearch` function of MATLAB® is as follows:

$$J = W_V\dot{V}^2 + W_\alpha\dot{\alpha}^2 + W_q\dot{q}^2 + W_\theta\dot{\theta}^2 \tag{19}$$

In the above equation W_V, W_α, W_q and W_θ are the weights of V, α, q and θ respectively. A two dimensional grid (α,θ) is set up with constant velocity and zero pitch rate. The thrust is varied to maintain a constant velocity leaving the flap and the elevator deflections as free parameters, that are varied in order to minimize the cost function defined by Eq. 19. Table 3 summarizes the grid setup and the optimization parameters for the estimation of the longitudinal trim envelope for Cessna Citation II. The trim envelope is comprised of only those grid points for which control inputs are within the bounds and the following conditions are satisfied:

$$\left|\dot{V}\right| \le 1\times10^{-4}\ [\mathrm{m/s^2}], \quad |\dot{\alpha}| \le 1\times10^{-4}\ [\mathrm{rad/s}], \quad |\dot{q}| \le 1\times10^{-4}\ [\mathrm{rad/s^2}], \quad \dot{\theta} \le 1\times10^{-4}\ [\mathrm{rad/s}] \tag{20}$$

Table 3. Parameters for the Longitudinal Trim Envelope Computation

Bounds	Grid Resolution	Cost Function Weights
$T \in [2241, 44482]$ [N] $\delta_f \in [0, 0.698]$ [rad] $\delta_e \in [-0.314, 0.279]$ [rad] $\alpha \in [-0.244, 0.244]$ [rad] $\theta \in [-0.523, 0.523]$ [rad] $q = 0$ [rad/s]	$\alpha_{res} = 0.01$ [rad] $\theta_{res} = 0.055$ [rad]	$W_V = 10$ (for nominal aircraft) $W_V = 0$ (for 100% tail loss) $W_\alpha = W_q = W_\theta = 10$

Another analytical approach is based on the specific aircraft dynamics model where the first three equations in Eq. 18 are set to zero and are solved simultaneously for the control inputs $\mathbf{u} = [T \quad \delta_e \quad \delta_f]$. Although, this approach is very efficient, it requires a specific dynamics model, where the system must be consistent i.e., the number of equations and the number of unknowns must be equal. The same two dimensional grid is used as stated above and the equations are solved simultaneously at each grid point.

Figure 13 shows the longitudinal trim envelope for Cessna Citation II at Mach 0.4 and sea level, estimated using both approaches. It can be seen, that part of the trim envelope $\{(\alpha_{min}, \theta_{min}), (\alpha_{max}, \theta_{max})\} = \{(-0.035, -0.028), (-0.015, 0.028)\}$ is missing when using the cost function minimization as displayed in the right plot. This is because the optimization routine got stuck at a local minima, yielding an incorrect solution. This possibility of being stuck at a locally optimal solution makes this method numerically intensive. However, unlike solving the equations simultaneously, minimization works for almost any sophisticated dynamics model and the system does not have to be consistent.

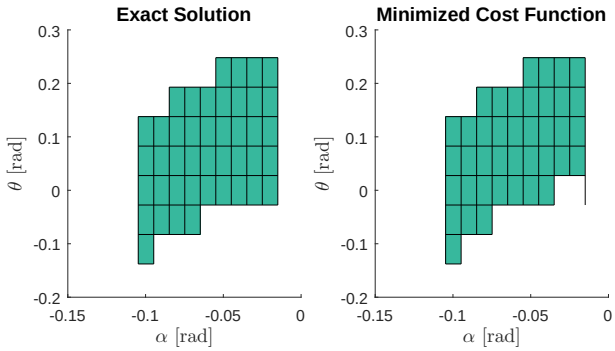

Figure 13. Longitudinal Trim Envelope for Nominal Cessna Citation II at Mach 0.4, Sea Level

Figure 14 shows the variation of the longitudinal trim envelope with different altitudes at Mach 0.4. As the altitude increases from sea level to 10,000 m, the trim envelope is shifting horizontally towards the right and vertically upward. This shift can be explained by the fact that as the altitude increases, density is decreasing and the magnitude of aerodynamic forces and moment are decreasing. Hence, an increase in the angle of attack is required to maintain the same aerodynamic forces and moment, such that the state derivatives are zero. Moreover, an increase in the angle of attack entails that the pitch angle is also increased in order to keep the gravitational force component constant, see Eq. 18.

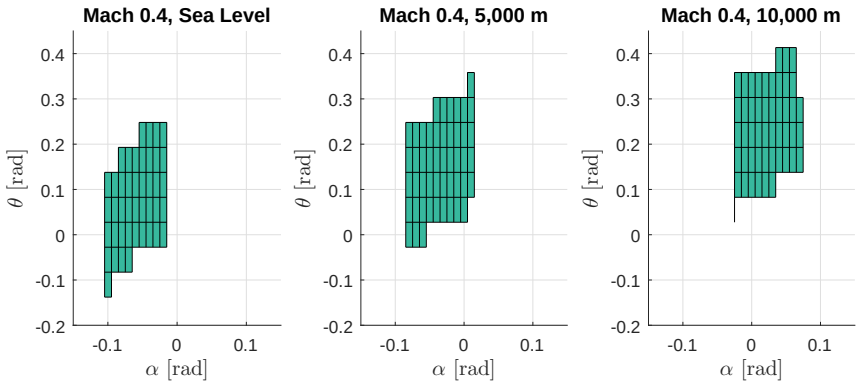

Figure 14. Longitudinal Trim Envelope for Nominal Cessna Citation II at Mach 0.4

Similarly, Figure 15 shows the variation of the longitudinal trim envelope with different Mach numbers at sea level. The trim envelope, on this occasion, is shifting towards the left and downwards. This opposite shifting behavior can be explained by the fact that as the Mach increases from 0.2 to 0.4 at the same altitude, the magnitude of aerodynamic forces and moment increase, and a decrease in the angle of attack is required to maintain the aerodynamic forces and moment. Also, the pitch angle has to be decreased in order to compensate for decreasing angle of attack in the gravitational force term.

Lastly, Figure 16 compares the longitudinal trim envelopes for the nominal aircraft and the damaged

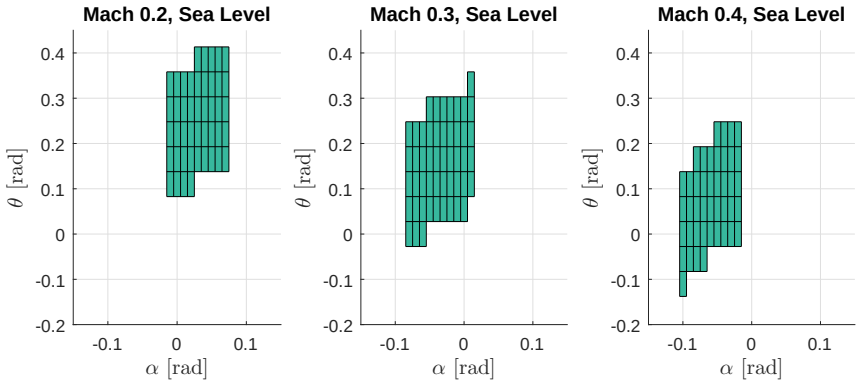

Figure 15. Longitudinal Trim Envelope for Nominal Cessna Citation II at Sea level

aircraft with 100% tail loss. The effect of the vertical tail damage alone, does not affect the longitudinal trim envelope significantly and therefore only the longitudinal trim envelope for 100% tail loss scenario is discussed. It can be seen, that the trim envelope has significantly shrunk. This is expected as the complete horizontal tail is lost, with no elevator deflection. Hence, even a slight variation in the angle of attack will induce an unstable pitching moment that cannot be compensated. The conditions imposed by Eq. 20 for the minimization of the cost function defined by Eq. 19 are too strict for trimming the damaged aircraft. Therefore, much more flexible conditions were imposed with $W_V = 0$.

$$\left|\dot{V}\right| \leq 1 \text{ [m/s}^2\text{]}, \quad |\dot{\alpha}| \leq 5 \times 10^{-2} \text{ [rad/s]}, \quad |\dot{q}| \leq 5 \times 10^{-2} \text{ [rad/s}^2\text{]}, \quad \dot{\theta} \leq 5 \times 10^{-2} \text{ [rad/s]} \tag{21}$$

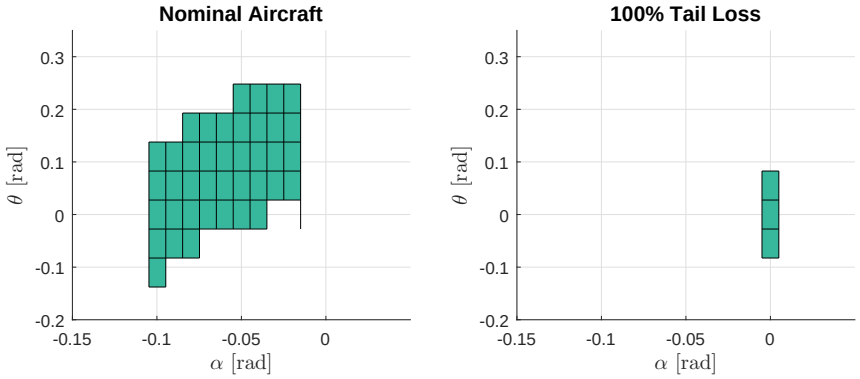

Figure 16. Longitudinal Trim Envelope for Cessna Citation II at Mach 0.4, Sea level

Figure 17 shows the contour plot of the longitudinal trim envelope for the damaged Cessna Citation II with 100% tail loss, shaded according to $\dot{V}$. It can be seen that the aircraft accelerates with pitch down and decelerates with pitch up motion. This acceleration and deceleration is due to the flexible condition on $\dot{V}$ as stated in Eq. 21. With an almost constant angle of attack, any change in pitch angle will require a change in thrust. However, change in the thrust is limited by the fact that the thrust is generating a pitch down motion. An increase in the thrust will cause the aircraft to pitch down or a decrease in the thrust may cause the aircraft to pitch up, and these pitching motions cannot be compensated.

V.B. Longitudinal Safe Flight Envelope

In section II, the safe flight envelope was defined as the intersection between the forward and the backward reachable sets. Forward or backward reachable set is computed by solving the HJB equation, Eq. 6, as an initial value or a terminal value problem respectively, to get the invariant set and then the principle of duality is utilized, Eq. 2, to obtain the reachability set. Eq. 6 is solved using the level set method toolbox.[19,20] The

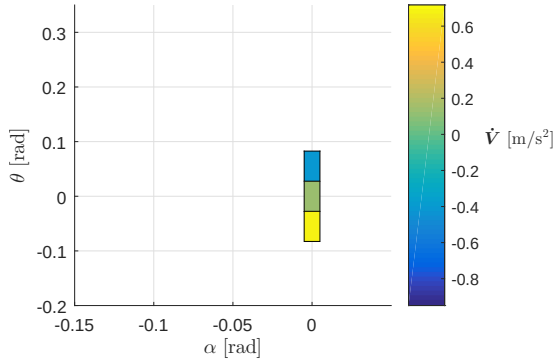

Figure 17. Longitudinal Trim Envelope shaded according to $\dot{V}$ for Damaged Cessna Citation II (100% Tail Loss) at Mach 0.4, Sea level

trim envelope K computed in the previous section is evolved over a time horizon T and is described by the following implicit function:

$$l(\mathbf{x}) = \min\{x_1 - \alpha_{min}, \alpha_{max} - x_1, x_2 - \theta_{min}, \theta_{max} - x_2, x_3 - q_{min}, q_{max} - x_3\} \tag{22}$$

The level set method requires at least one grid point inside the trim set, so that the implicit function can be evolved in time to get a meaningful reachable set. However, the longitudinal trim envelope K is a two dimensional plane (α, θ) with $q = 0$. Therefore, it is assumed, that the states in the near vicinity of $q = 0$ are also part of the trim set, to be specific $\{q \in K | \, |q| \leq 0.01\}$, which yields an implicit surface defined by Eq. 22. Moreover, it can be noticed that $l(\mathbf{x}) \geq 0$ for $\mathbf{x} \in K$ and $l(\mathbf{x}) < 0$ for $\mathbf{x} \notin K$. Table 4 outlines the parameters that are specified for the reachable set computation.

Table 4. Solver Settings for the Reachable Set Computation (Longitudinal Safe Flight Envelope)

Parameter	Setting
Computational Domain	$[-0.35, 0.35]\,\text{rad} \times [-0.785, 0.785]\,\text{rad} \times [-0.8, 0.8]\,\text{rad/s}$
Number of Grids	$100 \times 100 \times 100$
Time Horizon	1.0 s

The system defined by the last three equations of Eq. 18 results in a Hamiltonian function of Eq. 6:

$$H(\mathbf{p}, \mathbf{x}, \mathbf{u}) = p_1\dot{\alpha} + p_2\dot{\theta} + p_3\dot{q} \tag{23}$$

where $\mathbf{p}$ in the above equation are the co-states of the value function in Eq. 6: $p_1 = \frac{\partial V_2}{\partial \alpha}$, $p_2 = \frac{\partial V_2}{\partial \theta}$ and $p_3 = \frac{\partial V_2}{\partial q}$. The quantity to be minimized in the Hamiltonian of Eq. 23 becomes:

$$-p_1 C_{L_{\delta_e}} \delta_e \frac{\rho S}{2m} V - p_1 C_{L_{\delta_f}} \delta_f \frac{\rho S}{2m} V + p_3 C_{m_{\delta_e}} \delta_e \frac{\rho S \bar{c}}{2J_{yy}} V^2 \tag{24}$$

The minimizers, δ_e and δ_f, depend on the sign of the co-states p_1 and p_3. Recall that $V > 0$ and $C_{L_{\delta_f}} > 0$, then the optimal control inputs for minimizing the Hamiltonian are:

- $\delta_e = \begin{cases} \delta_{e_{\min}} & \text{if } p_3 C_{m_{\delta_e}} \frac{\rho S \bar{c}}{2J_{yy}} V - p_1 C_{L_{\delta_e}} \frac{\rho S}{2m} > 0 \\ \delta_{e_{\max}} & \text{if } p_3 C_{m_{\delta_e}} \frac{\rho S \bar{c}}{2J_{yy}} V - p_1 C_{L_{\delta_e}} \frac{\rho S}{2m} < 0 \\ [\delta_{e_{\min}}, \delta_{e_{\max}}] & \text{if } p_3 C_{m_{\delta_e}} \frac{\rho S \bar{c}}{2J_{yy}} V - p_1 C_{L_{\delta_e}} \frac{\rho S}{2m} = 0 \end{cases}$
- $\delta_f = \begin{cases} \delta_{f_{\min}} & \text{if } p_1 < 0 \\ \delta_{f_{\max}} & \text{if } p_1 > 0 \\ [\delta_{f_{\min}}, \delta_{f_{\max}}] & \text{if } p_1 = 0 \end{cases}$

whereas thrust T is varied, such that the velocity V is constant throughout the computational domain of the reachability analysis and is computed by setting the first equation of Eq. 18 to zero and solving for the thrust. The ranges of the control inputs are stated in Table 3.

Figure 18 shows the variation of the safe flight envelope with different Mach numbers at sea level for the time horizon $T = 1$ s. Clearly, with the increasing Mach and hence the dynamic pressure, the aircraft's maneuverability increases as shown by the increasing size of the safe flight envelope. Furthermore, it can be seen, that there is a noticeable difference between the forward and the backward reachable sets; there are states that can be reached within $T = 1$ s, however, coming back to the trim envelope from the same states is not possible, and vice versa. Another interesting fact to notice here, is that the backward reachable set encompasses and extends beyond the computational domain in the $\alpha - q$ plane. Similarly, the forward reachable set at Mach 0.4 and sea level, completely encompasses the $\theta - q$ plane. It is observed that the reachability set extends far from the region, where the linear aerodynamic model and/or structural limits are valid.

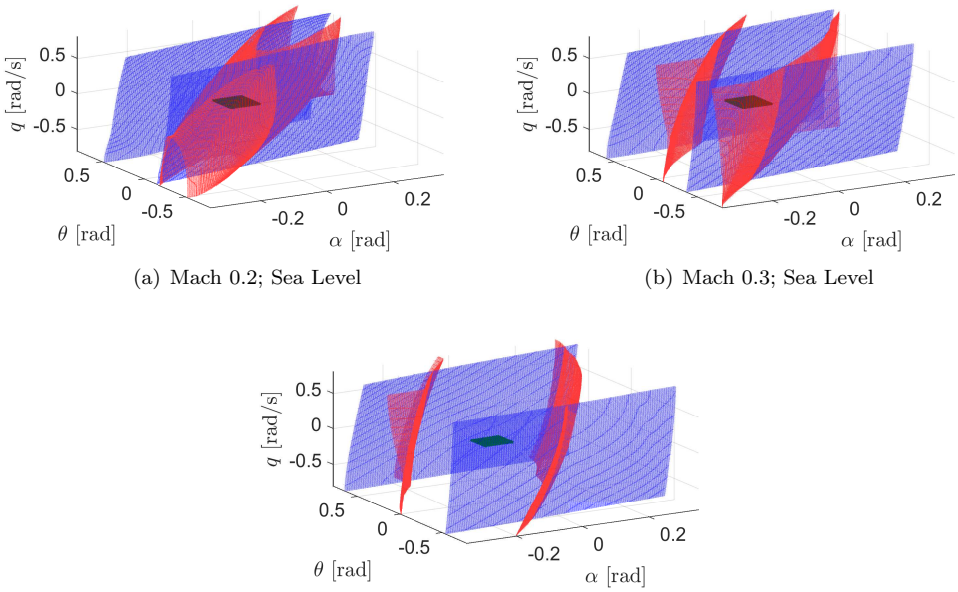

(a) Mach 0.2; Sea Level

(b) Mach 0.3; Sea Level

(c) Mach 0.4; Sea Level

Figure 18. Longitudinal Safe Flight Envelope for Nominal Cessna Citation II with $T = 1$ s (Variation with Mach), Green: Trim Envelope; Blue: Backward Reachable Set; Red: Forward Reachable Set

The variation of the safe flight envelope with different altitudes at Mach 0.4 is shown in Figure 19. As the altitude increases from sea level to 10,000 m, the safe flight envelope shrinks. With increasing altitude, density decreases and hence the dynamic pressure drops, which makes the aircraft less maneuverable.

The comparison of the safe flight envelopes for the nominal and the damaged Cessna Citation II is presented in Figure 20. An enormous reduction in the size of the safe flight envelope with the complete tail lost is visible. The backward and the forward reachable sets extend in the opposite direction in the $\alpha-$axis. As the elevator is lost, positive pitch angles and pitch rates are not reachable from the trim envelope. On the other hand, thrust is causing the aircraft to pitch down, which can be observed by the fact, that the forward reachable set is stretching towards negative pitch angles and pitch rates, however, coming back from these negative states is impossible as these states are not part of the backward reachable set. While thrust is fixed in order to maintain the velocity, the only control available is the flap deflection, giving a slight room for maneuverability in the angle of attack.

In order to quantify the change in the size of the safe flight envelopes, number of grid points inside the reachable set as a percentage of total grid points ($100 \times 100 \times 100$) is plotted against different flight conditions and tail damages in Figure 21. As can be seen, that the increase in percentage grid points inside the reachable set (forward and backward) is almost linear with increasing Mach. Similarly, the decrease in the size of the safe flight envelope is also nearly linear with altitude. Furthermore, the third plot in Figure 21 shows that the reachable sets for the 100% tail damage have shrunk remarkably and the percentage of grid points inside the reachable set has reduced to just 0.11%.

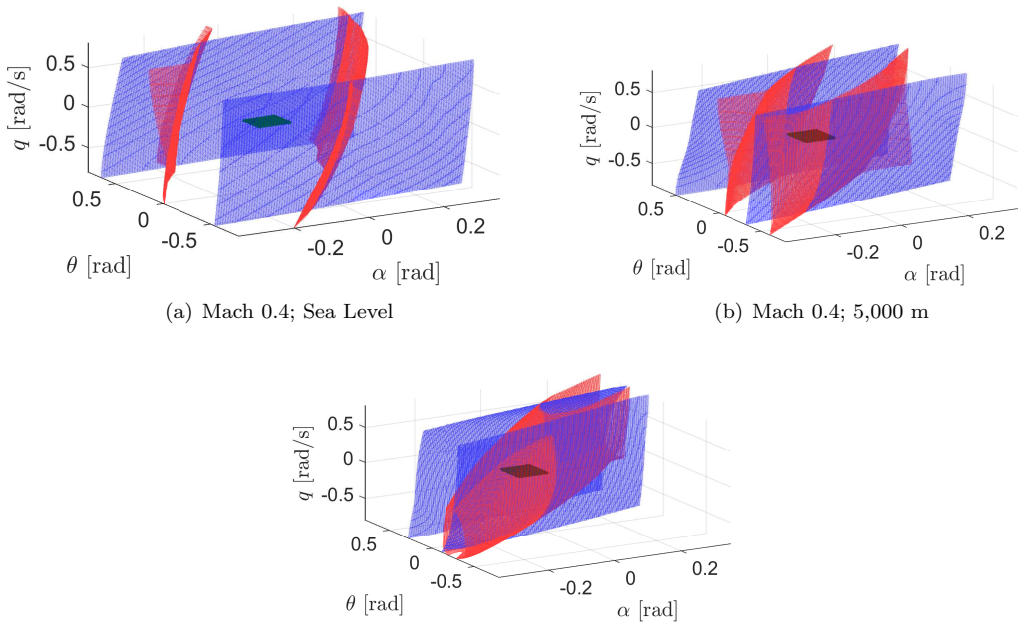

(a) Mach 0.4; Sea Level

(b) Mach 0.4; 5,000 m

(c) Mach 0.4; 10,000 m

Figure 19. Longitudinal Safe Flight Envelope for Nominal Cessna Citation II with $T = 1$ s (Variation with Altitude), Green: Trim Envelope; Blue: Backward Reachable Set; Red: Forward Reachable Set

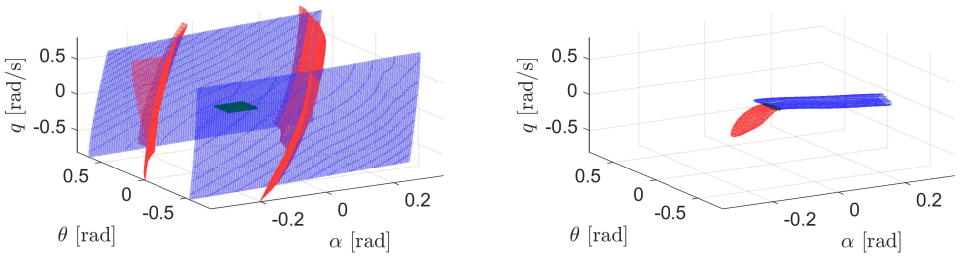

(a) Nominal Aircraft

(b) 100% Tail Loss

Figure 20. Longitudinal Safe Flight Envelope for Cessna Citation II with $T = 1$ s at Mach 0.4, Sea Level, Green: Trim Envelope; Blue: Backward Reachable Set; Red: Forward Reachable Set

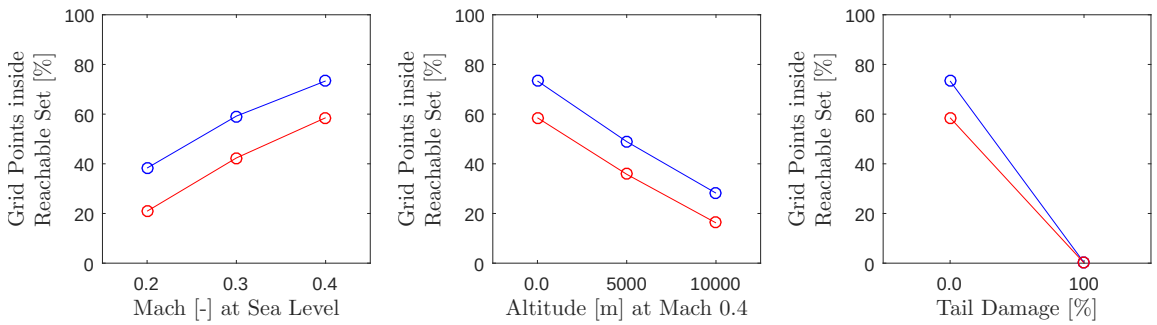

(a) Variation with Mach

(b) Variation with Altitude

(c) Vartiation with Tail Damage

Figure 21. Change in the Percentage of Grid Points inside the Longitudinal Reachable Set, Blue: Backward Reachable Set; Red: Forward Reachable Set

Table 5 lists the computational time for the reachability set analysis using the level set method applied to the three dimensional longitudinal dynamics. The computational time required for the forward and the backward reachable set is almost equal. However, it is interesting to see, that as the reachable set has shrunk with decreasing Mach or increasing altitude or for the damaged aircraft, so has the time for computing the respective reachable set.

Table 5. Computational Time* for the Longitudinal Reachability Set with $T = 1$ s

Damage Type	Flight Condition	$t_{\mathcal{F}}$ [s]	$t_{\mathcal{B}}$ [s]
Nominal	M 0.2, Sea level	1950.8	1961.9
	M 0.3, Sea level	2682.8	2697.2
	M 0.4, Sea level	4208.1	4178.0
	M 0.4, 5000 m	2409.2	2396.7
	M 0.4, 10000 m	1687.7	1639.0
100% VT Lost	M 0.4, Sea level	1211.3	1238.6

* Computation performed on a Core i5, 2.40GHz processor running Windows® 7 and MATLAB® R2015b.

In order to validate the computed reachable sets, two sets of Monte Carlo simulations have been performed. The first set considers randomly generated state trajectories initialized throughout the state space with constant control inputs all along the state trajectory. The second set considers a single trajectory constructed from sets of random candidate trajectories with arbitrary control inputs changing at each time step dt. Figure 22 illustrates the aforementioned Monte Carlo methods.

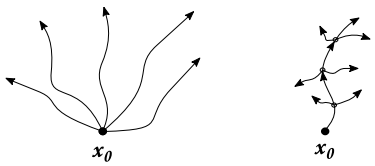

Figure 22. Illustration of Two Monte Carlo Simulation Methods: Random Trajectories with Constant Inputs (left) and A Single Trajectory Constructed from Sets of Candidate Increments (right)

As an example, a Monte Carlo simulation performed for backward reachability set with $q = 0$ at sea level and Mach 0.4 is presented in Figure 23. Trajectories are initialized on a 20×20 grid on the $\alpha - \theta$ plane. The left plot in Figure 23 shows the result of the Monte Carlo analysis performed with the first method. It can be seen that only a limited number of initial states near the trim envelope are verified as the backward reachable set using the random inputs that are fixed throughout the state trajectory. Plot on the right presents the result of Monte Carlo simulation implemented with the second method. This time almost all the states within the backward reachable set are verified. No state outside the backward reachable set is successful in initiating a state trajectory that lead to the trim envelope within the time horizon of $T = 1$ s. Although, the control inputs and the trajectories initiated by these inputs at each time step dt are randomly selected, most of the states are verified.

Figure 24 shows the variation of the control inputs and the states with time, as the state trajectory proceeds from an initial state to the trim envelope. The trajectory is initiated at $(\alpha, \theta, q) = (0.3132 \text{ rad}, 0.5371 \text{ rad}, 0 \text{ rad/s})$, which lies inside the backward reachable set. From this state, the trim envelope cannot be reached with a random input that is fixed throughout the trajectory within the given time horizon (Monte Carlo method 1). However, the trim envelope is reached within $t = 0.8$ s when the random input is changed at each time increment dt (Monte Carlo method 2). The top plot in Figure 24 shows the change in the flap and the elevator deflection as the state trajectory proceeds. The variation of thrust is shown in the second plot. As can be seen that after each increment $dt = 0.1$ s, the flap and the elevator deflection is arbitrarily changed, whereas the thrust is almost constant, since it is varied to maintain the velocity. The third plot shows the state trajectory itself. The aircraft undergoes extreme maneuvers in order to reach the trim envelope, with state changing at a very high rate i.e., after every 0.1 s. It can be concluded, that although the reachability analysis accurately computes the safe flight envelope, few of the

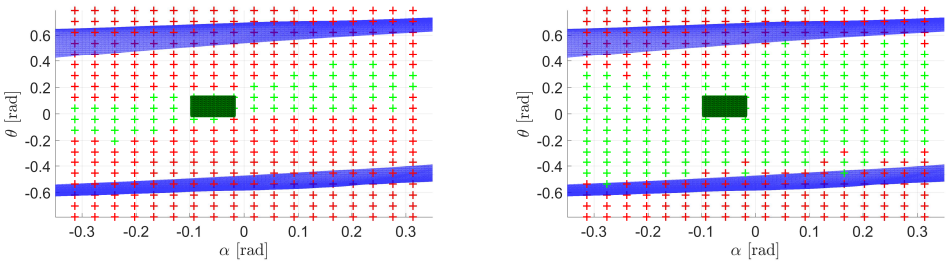

(a) Monte Carlo with Fixed Arbitrary Inputs (b) Monte Carlo with Incremental Inputs

Figure 23. Monte Carlo Analysis for Backward Reachable Set (Nominal Cessna Citation II) with $T = 1$ s at Mach 0.4, Sea Level, Green: Successful; Red: Unsuccessful

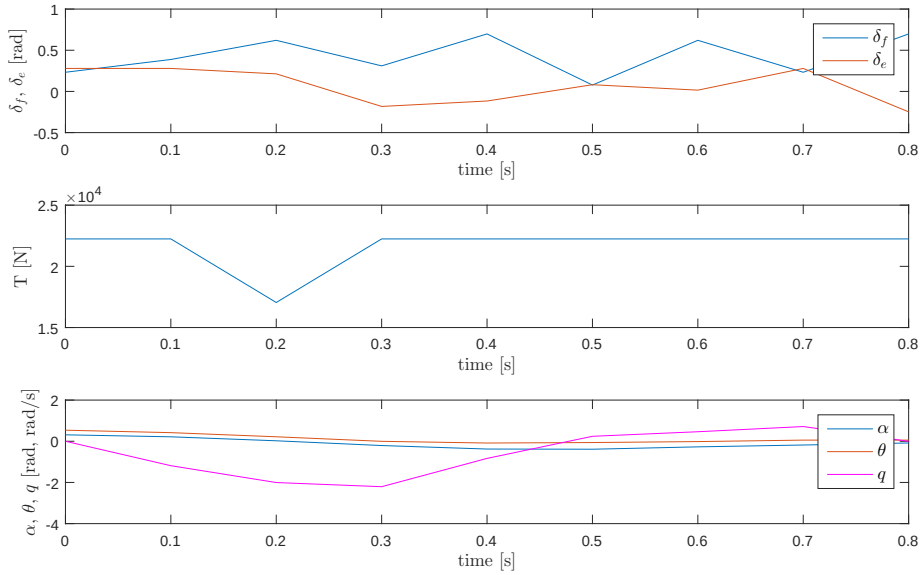

Figure 24. Control Input Variation and State Trajectory for Nominal Cessna Citation II initialized at $(\alpha, \theta, q) = (0.3132$ rad, 0.5371 rad, 0 rad/s$)$ at Mach 0.4, Sea Level

states that are part of the "theoretical" reachable set (forward or backward) may not be reachable in reality. This is due to the fact, that the pilot may not be able to fly such a complex maneuver or the trajectory passes through the states that lie outside the aerodynamic and/or structural limits of the aircraft.

VI. Lateral Envelope

Roll, yaw and sideslip define the lateral motion of an aircraft. The state variables that characterize the lateral motion are: velocity V, sideslip β, roll rate p, yaw rate r and roll angle ϕ. Since no longitudinal motion is involved, therefore $q = \dot{q} = 0$, whereas the angle of attack α and the pitch angle θ are fixed with $\dot{\alpha} = \dot{\theta} = 0$. With these conditions, Eqs. 8, 7 and 9 can be reduced to lateral equations of motion:

$$\begin{cases} \dot{V} = \dfrac{1}{m}\left(T\cos\alpha\cos\beta - \frac{1}{2}\rho V^2 S C_D(\alpha) + mg_1\right) \\ \dot{\beta} = p\sin\alpha - r\cos\alpha + \dfrac{1}{mV}\left[-T\cos\alpha\sin\beta + \frac{1}{2}\rho V^2 S C_Y(\alpha,\beta,p,\delta_r) + mg_2\right] \\ \dot{p} = \dfrac{1}{J_{xx}J_{zz} - J_{zx}^2}\left(J_{zz}\frac{1}{2}\rho V^2 S b C_l(\alpha,\beta,p,r,\delta_a,\delta_r) + J_{zx}\frac{1}{2}\rho V^2 S b C_n(\alpha,\beta,p,r,\delta_a,\delta_r)\right) \\ \dot{r} = \dfrac{1}{J_{xx}J_{zz} - J_{zx}^2}\left(J_{zx}\frac{1}{2}\rho V^2 S b C_l(\alpha,\beta,p,r,\delta_a,\delta_r) + J_{xx}\frac{1}{2}\rho V^2 S b C_n(\alpha,\beta,p,r,\delta_a,\delta_r)\right) \\ \dot{\phi} = p + r\frac{\sin\theta}{\cos\theta}\cos\phi \end{cases} \tag{25}$$

In the above set of equations, g_1 and g_2 are the components of gravity vector and were presented in section III.

VI.A. Lateral Trim Envelope

The lateral trim envelope is computed by minimizing the following cost function for some fixed states:

$$J = W_V \dot{V}^2 + W_\beta \dot{\beta}^2 + W_p \dot{p}^2 + W_r \dot{r}^2 + W_\phi \dot{\phi}^2 \tag{26}$$

For the current research, a one dimensional (β) trim envelope has been computed with $p = r = \phi = 0$ at a fixed longitudinally trimmed angle of attack α_{trim} and pitch angle θ_{trim}, see Table 6. The parameters for the lateral trim envelope computation for Cessna Citation II are listed in Table 7. Sideslip angle is considered trimmed, if the inputs are within the bounds and the following conditions are satisfied:

$$\begin{gathered} \left|\dot{V}\right| \leq 1 \times 10^{-4} \text{ [m/s}^2\text{]}, \quad \left|\dot{\beta}\right| \leq 0.05 \text{ [rad/s]}, \\ |\dot{p}| \leq 1 \times 10^{-4} \text{ [rad/s}^2\text{]}, \quad |\dot{r}| \leq 1 \times 10^{-4} \text{ [rad/s}^2\text{]}, \quad \dot{\phi} \leq 1 \times 10^{-4} \text{ [rad/s]} \end{gathered} \tag{27}$$

Table 6. Fixed Longitudinal Trim States used for Lateral Trim Computation

Flight Condition	$(\alpha_{trim}, \theta_{trim})$ [rad]
Mach 0.2, Sea level	$(0.005, 0.1)$
Mach 0.3, Sea level	$(-0.005, 0.05)$
Mach 0.4, Sea level	$(-0.0249, 0)$
Mach 0.4, 5,000 m	$(-0.005, 0.05)$
Mach 0.4, 10,000 m	$(0.005, 0.1)$

Table 7. Parameters for the Lateral Trim Envelope Computation

Bounds	Grid Resolution	Cost Function Weights
$T \in [2241, 44482]$ [N] $\delta_a \in [-0.5934, 0.5934]$ [rad] $\delta_r \in [-0.3840, 0.3840]$ [rad] $\beta \in [-0.3491, 0.0.3491]$ [rad] $p = r = 0$ [rad/s] $\phi = 0$ [rad]	$\beta_{res} = 0.007$ [rad]	$W_V = W_\beta = W_p = W_r = W_\phi = 10$

The trimmed sideslip angle for the nominal Cessna Citation II at various flight conditions has been presented in Figure 25. Similarly, Figure 26 shows a comparison of lateral trim set for different damage cases at Mach 0.4 and sea level. No major change is observed, either with the flight condition or with the vertical tail damage. However, a slight decrease can be noticed in the trim set for the damaged Cessna Citation II with 75% vertical tail loss. The almost unvarying behavior of the trim set with the changing flight conditions is due to the fact, that the condition imposed on the rate of sideslip angle $\dot{\beta}$ (Eq. 27) is not very strict. Moreover, although the rudder control effectiveness is decreasing with the spanwise damage to the vertical tail, the side force Y generated by the sideslip is also decreasing, allowing the aircraft to trim at almost the same sideslip angle.

VI.B. Lateral Safe Flight Envelope

A two dimensional ($\beta - r$) safe flight envelope is computed with $\dot{p} = p = \dot{\phi} = \phi = 0$ by evolving the trim set K forward and backwards in time. By considering the states in the proximity of $r = 0$ to be part of the trim set i.e., $\{r \in K | \, |r| \leq 0.01\}$, the following implicit function is defined:

$$l(\mathbf{x}) = \min\{x_1 - \beta_{min}, \beta_{max} - x_1, x_2 - r_{min}, r_{max} - x_2\} \tag{28}$$

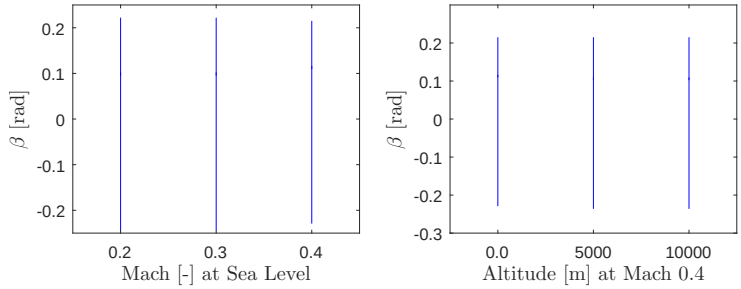

Figure 25. Lateral Trim Set for Nominal Cessna Citation II at various Flight Conditions

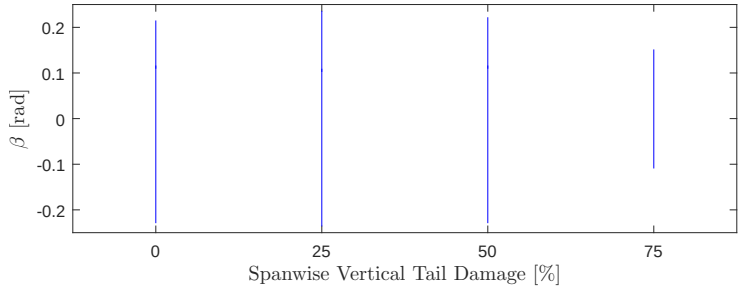

Figure 26. Lateral Trim Set for Cessna Citation II at Mach 0.4, Sea Level

Here as well, it can be noticed that $l(\mathbf{x}) \geq 0$ for $\mathbf{x} \in K$ and $l(\mathbf{x}) < 0$ for $\mathbf{x} \notin K$. Table 8 outlines the parameters that are assigned for the two dimensional reachable set computation.

Table 8. Solver Settings for the Reachable Set Computation (Lateral Safe Flight Envelope)

Parameter	Setting
Computational Domain	$[-1.05, 1.05]\,\text{rad} \times [-1.0, 1.0]\,\text{rad/s}$
Number of Grids	200×200
Time Horizon	1.0 s

The Hamiltonian function in Eq. 6 for the lateral safe flight envelope computation is defined as:

$$H(\mathbf{p}, \mathbf{x}, \mathbf{u}) = p_1\dot{\beta} + p_2\dot{r} \tag{29}$$

where the co-states in the above equation are: $p_1 = \frac{\partial V_2}{\partial \beta}$ and $p_2 = \frac{\partial V_2}{\partial r}$. With the aileron deflection δ_a being varied to prevent the aircraft from rolling and thrust T to maintain the constant velocity, the only minimizer in the Hamiltonian function in Eq. 29 is the rudder deflection δ_r, which yields the following quantity to be minimized in the Hamiltonian function:

$$p_1 \frac{\rho S}{2m} V C_{Y_{\delta_r}} \delta_r + p_2 \frac{\rho S b}{2(J_{xx}J_{zz} - J_{zx}^2)} V^2 \left(J_{zx} C_{l_{\delta_r}} + J_{xx} C_{n_{\delta_r}}\right) \delta_r \tag{30}$$

Then the optimal rudder deflection to minimize the Hamiltonian function becomes straightforward:

- $\delta_r = \begin{cases} \delta_{r_{min}} & \text{if } p_1 \frac{\rho S}{2m} V C_{Y_{\delta_r}} + p_2 \frac{\rho S b}{2(J_{xx}J_{zz} - J_{zx}^2)} V^2 \left(J_{zx} C_{l_{\delta_r}} + J_{xx} C_{n_{\delta_r}}\right) > 0 \\ \delta_{r_{max}} & \text{if } p_1 \frac{\rho S}{2m} V C_{Y_{\delta_r}} + p_2 \frac{\rho S b}{2(J_{xx}J_{zz} - J_{zx}^2)} V^2 \left(J_{zx} C_{l_{\delta_r}} + J_{xx} C_{n_{\delta_r}}\right) < 0 \\ [\delta_{r_{min}}, \delta_{r_{max}}] & \text{if } p_1 \frac{\rho S}{2m} V C_{Y_{\delta_r}} + p_2 \frac{\rho S b}{2(J_{xx}J_{zz} - J_{zx}^2)} V^2 \left(J_{zx} C_{l_{\delta_r}} + J_{xx} C_{n_{\delta_r}}\right) = 0 \end{cases}$

The required aileron deflection δ_a to keep the aircraft level is computed by setting $\dot{p} = 0$ in Eq. 25 and solving for δ_a. Moreover, the required thrust T is computed by setting $\dot{V} = 0$ in Eq. 25 and solving for T.

Figures 27 and 28 shows the variation of the lateral safe flight envelope with different flight conditions. As expected, the safe flight envelope grows as the velocity of the aircraft increases, shown in Figure 27.

Additionally, the safe flight envelope shrinks as the altitude increases from sea level to 10,000 m, see Figure 28. An interesting fact to notice here is that the effect of decreasing the Mach by 0.1 and increasing the altitude by 5,000 m is almost the same on the lateral safe flight envelope of Cessna Citation II.

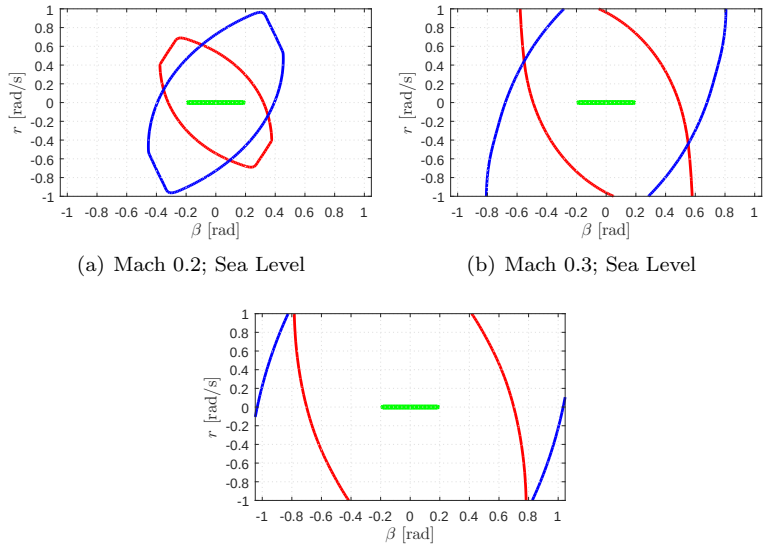

(a) Mach 0.2; Sea Level (b) Mach 0.3; Sea Level

(c) Mach 0.4; Sea Level

Figure 27. Lateral Safe Flight Envelope for Nominal Cessna Citation II with $T = 1$ s (Variation with Mach), Green: Trim Envelope; Blue: Backward Reachable Set; Red: Forward Reachable Set

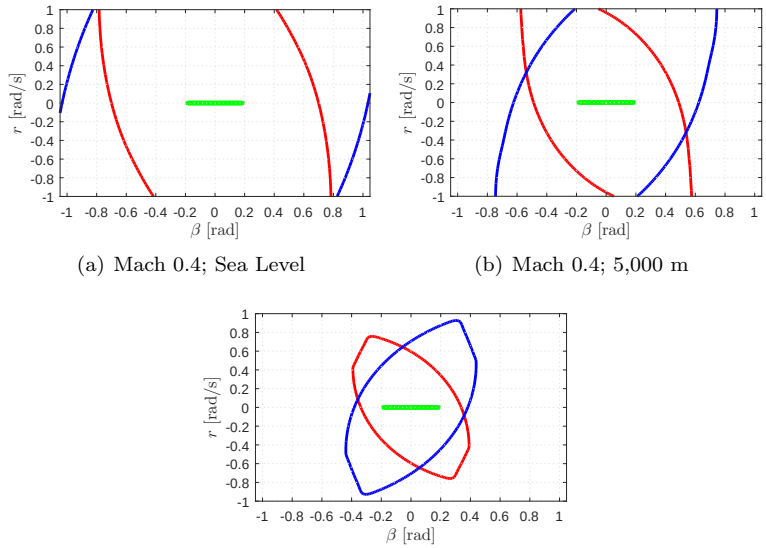

(a) Mach 0.4; Sea Level (b) Mach 0.4; 5,000 m

(c) Mach 0.4; 10,000 m

Figure 28. Lateral Safe Flight Envelope for Nominal Cessna Citation II with $T = 1$ s (Variation with Altitude), Green: Trim Envelope; Blue: Backward Reachable Set; Red: Forward Reachable Set

Figure 29 shows the lateral safe flight envelopes for Cessna Citation II for various vertical tail damages at Mach 0.4 and sea level. As the percentage of spanwise vertical tail damage increases, the safe flight envelope shrinks. The range of sideslip angle β in the forward and the backward reachable sets decreases with the vertical tail damage. However, the yaw rate r range is almost the same for various damages. This shrinking in the safe flight envelope is unlike the shrinking in the safe flight envelope due to different flight conditions. At higher altitude and lower Mach numbers, the overall maneuvering capability of the aircraft decreases and the aircraft cannot simply reach high sideslip angles and high yaw rates. On the contrary, due to spanwise vertical tail damage the aircraft can reach to or comeback from high sideslip angles but at high yaw rates.

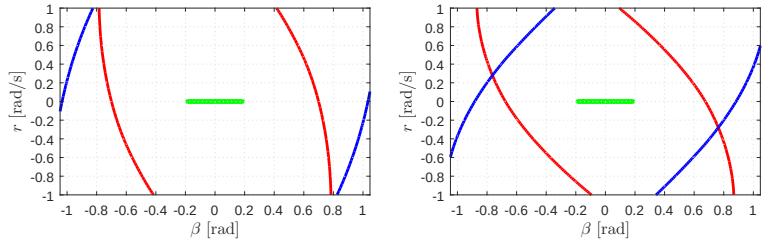

(a) Nominal Aircraft

(b) 25% VT Loss

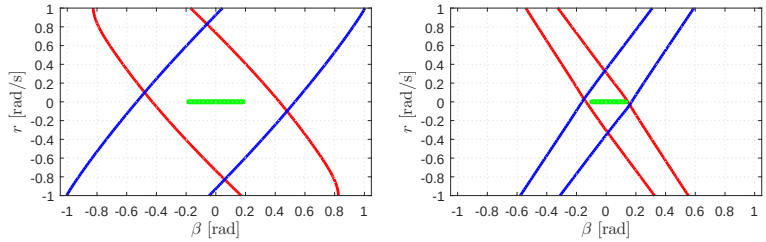

(c) 50% VT Loss

(d) 75% VT Loss

Figure 29. Lateral Safe Flight Envelope for Cessna Citation II with $T = 1$ s at Mach 0.4, Sea Level, Green: Trim Envelope; Blue: Backward Reachable Set; Red: Forward Reachable Set

In addition to understanding the effects of various structural damages and flight conditions on the safe flight envelope, it is also very important to know that how different time horizons would affect the safe flight envelope of an aircraft. Figure 30 presents the safe flight envelopes for nominal Cessna Citation II at Mach 0.4 and sea level for three different time horizons. As expected, the safe flight envelope expands as the time horizon is increased. As the time horizon decreases, the lateral safe flight envelope shrinks in $\beta-$axis i.e., a limited range of sideslip angle is reachable with almost same yaw rate r, unlike the safe flight envelope for the damaged vertical tail, where higher sideslip angles were reachable, however, at higher yaw rates.

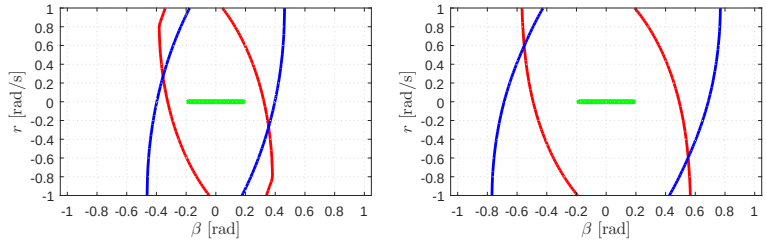

(a) $T = 0.5$ s

(b) $T = 0.75$ s

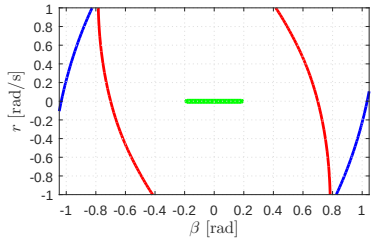

(c) $T = 1.0$ s

Figure 30. Lateral Safe Flight Envelope for Nominal Cessna Citation II at Mach 0.4, Sea Level (Variation with Time Horizon), Green: Trim Envelope; Blue: Backward Reachable Set; Red: Forward Reachable Set

The changes in the lateral safe flight envelope due to different flight conditions, vertical tail damages and time horizons are summarized in Figure 31. With different flight conditions, the change in the lateral safe

flight envelope has the same behavior as in the longitudinal safe flight envelope i.e., the safe flight envelope changes almost linearly with different flight conditions as suggested by results presented in the top two plots. Figure 31(c) shows that the reachable set expands with increasing time horizon T. The shrinkage in the reachability sets with the vertical tail damage is shown in Figure 31(d). The percentage of grid points inside the reachable set decreases with increasing spanwise vertical tail damage as expected, however, this damage is not linear.

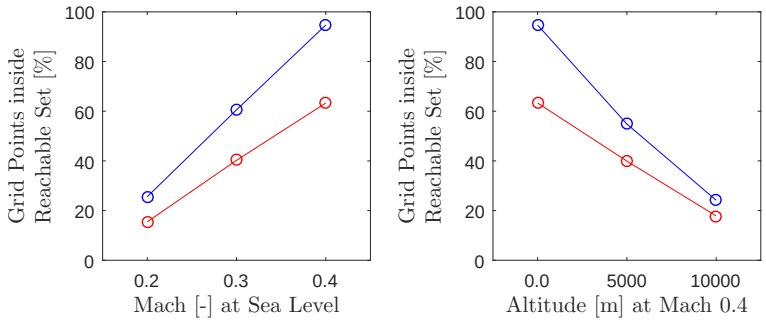

(a) Variation with Mach (Nominal Aircrat with $T = 1$ s)

(b) Variation with Altitude (Nominal Aircrat with $T = 1$ s)

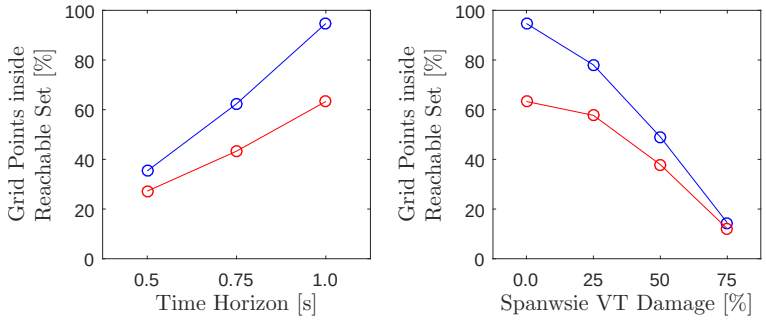

(c) Vartiation with Time Horizon (Nominal Aircrat at Mach 0.4, Sea Level)

(d) Vartiation with Vertical Tail Damage (Mach 0.4, Sea Level with $T = 1$ s)

Figure 31. Change in the Percentage of Grid Points inside the Lateral Reachable Set, Blue: Backward Reachable Set; Red: Forward Reachable Set

In order to demonstrate the feasibility of the database approach, variation of the number of grid points inside the reachable set with spanwise vertical tail damage, Figure 31(d), has been fit with a quadratic polynomial model. Two spanwise vertical tail damages are investigated in order to substantiate the hypothesis of interpolatibility. Table 9 shows the comparison between the number of grid points inside the reachable set computed using the level set method and the second order polynomial interpolation. For both damages, it can be seen that the quadratic polynomial interpolation has approximated the number of grid points inside the reachable set fairly close to the actual results obtained by the level set method for both backward and forward reachable sets. The idea of interpolation in the database approach is corroborated by the comparison presented in Table 9.

Similarly, the variation of the number of grid points inside the reachable set with Mach number and altitude has been fit with a linear polynomial model. One trial Mach number and one altitude level is investigated. Table 10 presents the comparison between actual and approximated number of grid points inside the reachable set. Here as well, the premise of interpolation between flight conditions within the database has been verified.

Lastly, the computational time for the reachability analysis applied to the two dimensional lateral dynamics is presented in Table 11. The time to compute the reachable set for the nominal Cessna Citation II at Mach 0.4 and sea level is largest. But with 25% vertical tail damage, the computational time decreases. However, as the vertical tail damage is further increased, so does the computational time. Comparing the computational time for the two dimensional reachability problem, Table 11, with the computational time

Table 9. Comparison of Level Set Method and Interpolation with Quadratic Polynomial Model at Mach 0.4, Sea Level with $T = 1$ s

Damage Type	Reachability Set	No. of Grid Points inside Reachable Set		Error
		Actual	2nd Order Approx.	
40% VT Lost	Forward	17882	18912	5.76 %
	Backward	23208	24759	6.68 %
60% VT Lost	Forward	11976	11745	-1.9 %
	Backward	15306	14699	-3.9 %

Table 10. Comparison of Level Set Method and Interpolation with Linear Polynomial Model for Nominal Cessna Citation II with $T = 1$ s

Flight Condition	Reachability Set	No. of Grid Points inside Reachable Set		Error
		Actual	1st Order Approx.	
Mach 0.35, Sea Level	Forward	20966	20646	-1.53 %
	Backward	31922	31018	-2.83 %
Mach 0.4, 7500 m	Forward	11062	11598	4.84 %
	Backward	15380	16105	4.7 %

for the three dimensional reachability problem presented in Table 5, demonstrates the inherent problem of "curse of dimensionality" with the reachability problem. The maximum computational time for the two dimensional lateral reachability problem with 200×200 grid and $T = 1$ s is less than two minutes. On the other hand, the maximum computational time for the three dimensional longitudinal reachability problem with $100 \times 100 \times 100$ grid and $T = 1$ s is seventy minutes.

Table 11. Computational Time for the Lateral Reachability Set with $T = 1$ s

Damage Type	Flight Condition	$t_{\mathcal{F}}$ [s]	$t_{\mathcal{B}}$ [s]
Nominal	M 0.2, Sea level	37.89	38.59
	M 0.3, Sea level	67.14	68.45
	M 0.4, Sea level	105.79	109.33
	M 0.4, 5000 m	64.86	64.82
	M 0.4, 10000 m	38.22	38.36
25% VT Lost	M 0.4, Sea level	46.94	46.34
50% VT Lost	M 0.4, Sea level	52.99	49.76
75% VT Lost	M 0.4, Sea level	78.46	69.72

VII. Conclusion

In order to investigate the feasibility of the novel database approach for online flight envelope prediction and protection, a three dimensional longitudinal and a two dimensional lateral safe flight envelope for the nominal and the damaged Cessna Citation II at various flight conditions was computed and presented in this paper. For the purpose of decoupling the dynamics, symmetrical damages with spanwise vertical tail damage were considered.

The safe flight envelopes were computed by defining a nonlinear reachability problem and solving it with the level set method through an optimal control formulation using actual aircraft control surface inputs. Nonlinear reachability analysis require a flight dynamics based physical model of an aircraft. Therefore, a simple method to identify the physical parameters of the aircraft (mass, inertia etc.) was presented.

Moreover, the aerodynamic stability and control derivatives were estimated using Digital Datcom.

It was shown that although the principle of time scale separation is very useful to solve the problem of "curse of dimensionality" in the reachability analysis for the slower dynamics, it is not feasible to implement the same principle for the reachability computation for faster dynamics when only considering the aircraft control surfaces as inputs.

By analyzing both longitudinal and lateral safe flight envelopes, it was observed, that the reachability set extends far beyond the region, where the linear aerodynamic model and the structural limits are valid. Introducing the aerodynamic model and structural limits will help restrict the computational domain. Moreover, it was also observed, that the reachability analysis computes a safe flight envelope that is "theoretically" reachable, however, practically it might not be possible to reach such a state due to a high rate of control input or maneuver requirement that is out of pilot's bandwidth.

It was demonstrated that the flight conditions have same effect on the longitudinal and the lateral safe flight envelopes. The safe flight envelope expands almost linearly with increasing Mach while it also shrinks linearly, with increasing altitude. This result is consistent with the fact that with an increasing Mach, the maneuverability of an aircraft increases, whereas the maneuverability decreases with increasing altitude. Similarly, the effects of various time horizons on the safe flight envelope were also presented. It was shown that the safe flight envelope grows as the time horizon is increased.

Furthermore, the lateral safe flight envelopes for the Cessna Citation II with 0%, 25%, 50% and 75% vertical tail loss, were compared. The comparison was quantified by the number of grid points inside the backward and the forward reachable sets. The results show that the number of grid points inside the reachable set decline almost quadratically with increasing spanwise vertical tail damage. A second order polynomial model was fitted on this data and then two candidate vertical tail damages were interpolated using this quadratic polynomial model. The same idea of interpolation, was also verified for different flight conditions by using a linear regression model. The comparison between the actual and the approximated grid points inside the reachable set show promising results and support the hypothesis of interpolatibility in the database approach.

It was further demonstrated, that different flight conditions, various time horizons and the vertical tail damages have different effects on the safe flight envelope. However, a unique trend can be observed for each of these categories.

At this moment, only the symmetrical damages have been considered. Future work will extend to asymmetrical damages. It should be noted, however, that in case of asymmetrical damages, the decomposition of the flight dynamics into longitudinal and lateral dynamics will be no longer valid and a nine dimensional safe flight envelope for fast dynamics will have to be computed. Therefore, a more computationally efficient method has to be explored, such that the higher dimensional safe flight envelopes can be computed offline and a database of these safe flight envelopes for various damages at different flight conditions can be constructed and analyzed. Moreover, future work will also include extensive and in-depth research in physical modeling (mass and inertia model, aerodynamic model etc.) of the damaged aircraft. Another topic for the further research is damage and failure identification and classification.

References

[1]Boeing, "Statistical Summary of Commercial Jet Airplane Accidents - Worldwide Operations 1959 - 2011," Technical report, Aviation Safety, Boeing Commercial Airplanes, Seattle, WA 98124-2207, 2012.

[2]Lopez, I. and Sarigul-Klijn, N., "A review of uncertainty in flight vehicle structural damage monitoring, diagnosis and control: Challenges and opportunities," *Progress in Aerospace Sciences*, Vol. 46, No. 7, October 2010, pp. 247–273.

[3]Lombaerts, T. J. J., *Fault Tolerant Flight Control - A Physica Model Approach*, Ph.D. dissertation, Faculty of Aerospace Engineering, Delft University of Technology, May 2010.

[4]Stroosma, O., Smaïli, H., Lombaerts, T., and Mulder, J. A., "Piloted Simulator Evaluation of New Fault-Tolerant Flight Control Algorithms for Reconstructed Accident Scenarios," *AIAA Modeling and Simulation Technologies Conference and Exhibit*, August 2008.

[5]Lombaerts, T., Schuet, S., Acosta, D. M., Kaneshige, J., Shish, K. H., and Martin, L., "Piloted Simulator Evaluation of Maneuvering Envelope Information for Flight Crew Awareness," *AIAA Guidance, Navigation, and Control Conference, AIAA SciTech*, 2015.

[6]Goman, M. G., Khramtsovsky, A. V., and Kolesnikov, E. N., "Evaluation of Aircraft Performance and Maneuverability by Computation of Attainable Equilibrium Sets," *Journal of Guidance, Control and Dynamics*, Vol. 31, No. 2, April–May 2008, pp. 329–339.

[7]Keller, J. D., McKillip, R. M., and Kim, S., "Aircraft Flight Envelope Determination using Upset Detection and Physical Modeling Methods," *AIAA Guidance, Navigation, and Control Conference*, August 2009.

[8]Menon, P. K., Sengupta, P., Vaddi, S., Yang, B.-J., and Kwan, J., "Impaired Aircraft Performance Envelope Estimation," *Journal of Aircraft*, Vol. 50, No. 2, 2013, pp. 410–424.

[9]Kitsios, I. and Lygeros, J., "Launch-Pad Abort Flight Envelope Computation for a Personnel Launch Vehicle Using Reachability," *AIAA Guidance, Navigation, and Control Conference and Exhibit*, August 2005.

[10]Seube, N. and Moitie, R., "Viability Analysis of an Aircraft Flight Domain for Take-Off in a Windshear," *Mathematical and Computer Modelling*, Vol. 36, No. 6, October 2002, pp. 633–641.

[11]van Oort, E. R., Chu, Q. P., and Mulder, J. A., "Maneuver Envelope Determination through Reachability Analysis," *Advances in Aerospace Guidance, Navigation and Control: Selected Papers of the 1st CEAS Specialist Conference on Guidance, Navigation and Control*, Springer Berlin Heidelberg, 2011, pp. 91–102.

[12]Tang, L., Roemer, M., Ge, J., Crassidis, A., Prasad, J. V. R., and Belcastro, C., "Methodologies for Adaptive Flight Envelope Estimation and Protection," *AIAA Guidance, Navigation, and Control Conference*, August 2009.

[13]Zhang, Y., de Visser, C. C., and Chu, Q. P., "Online Safe Flight Envelope Prediction for Damaged Aircraft: A Database-driven Approach," *AIAA Modeling and Simulation Technologies Conference, AIAA SciTech*, January 2016.

[14]Zhang, Y., de Visser, C. C., and Chu, Q. P., "Online Physical Model Identification for Database-driven Safe Flight Envelope Prediction of Damaged Aircraft," *AIAA Atmospheric Flight Mechanics Conference, AIAA SciTech*, January 2016.

[15]Anderson, J. D., *Aircraft Performance and Design*, McGraw-Hill Education, 1st ed., December 1998.

[16]Ruijgrok, G. J. J., *Elements of Airplane Performance*, Delft University Press, 2nd ed., 2007.

[17]van Oort, E. R., *Adaptive Backstepping Control and Safety Analysis for Modern Fighter Aircraft*, Ph.D. dissertation, Faculty of Aerospace Engineering, Delft University of Technology, June 2011.

[18]Lygeros, J., "On Reachability and Minimum Cost Optimal Control," *Automatica*, Vol. 40, No. 6, June 2004, pp. 917–927.

[19]Mitchell, I. and Tomlin, C. J., "Level Set Methods for Computation in Hybrid Systems," *Hybrid Systems: Computation and Control, Lecture Notes in Computer Science*, Vol. 1790, March 2000, pp. 310–323.

[20]Mitchell, I., Bayen, A. M., and Tomlin, C. J., "Validating a Hamilton-Jacobi Approximation to Hybrid System Reachable Set," *Hybrid Systems: Computation and Control, Lecture Notes in Computer Science*, March 2001, pp. 418–432.

[21]Osher, S. and Fedkiw, R., *Level Set Methods and Dynamic Implicit Surfaces*, Vol. 153 of *Applied Mathematical Sciences*, Springer-Verlag New York, 1st ed., January 2003.

[22]Lygeros, J., "Minimum Cost Optimal Control: An Application to Flight Level Tracking," *Mediterranean Conference on Control and Automation*, Rhodes, Greece, June 2003.

[23]Schuet, S., Lombaerts, T., Acosta, D., Wheeler, K., and Kaneshige, J., "An Adaptive Nonlinear Aircraft Maneuvering Envelope Estimation Approach for Online Applications," *AIAA Guidance, Navigation, and Control Conference, AIAA SciTech*, January 2014.

[24]Lombaerts, T. J. J., Schuet, S. R., Wheeler, K. R., Acosta, D. M., and Kaneshige, J. T., "Safe Maneuvering Envelope Estimation Based on a Physical Approach," *AIAA Guidance, Navigation, and Control Conference*, August 2013.

[25]Marco, A. D., Duke, E. L., and Berndt, J. S., "A General Solution to the Aircraft Trim Problem," *AIAA Modeling and Simulation Technologies Conference and Exhibit*, August 2007.

[26]Yi, G. and Atkins, E. M., "Methods of Trim State Discovery," *3rd International Symposium on Systems and Control in Aeronautics and Astronautics (ISSCAA)*, June 2010, pp. 654 – 659.

[27]van Kampen, E., Chu, Q. P., Mulder, J. A., and van Emden, M. H., "Nonlinear Aircraft Trim using Interval Analysis," *AIAA Guidance, Navigation, and Control Conference and Exhibit*, August 2007.

[28]Ananthkrishnan, N. and Sinha, N. K., "Level Flight Trim and Stability Analysis using Extended Bifurcation and Continuation Procedure," *Journal of Guidance, Control and Dynamics*, Vol. 24, No. 6, 2001, pp. 1225–1228.

[29]Stapel, J. C. J., de Visser, C. C., Chu, Q. P., and van Kampen, E., "Efficient Methods for Flight Envelope Estimation through Reachability Analysis," *AIAA Guidance, Navigation, and Control Conference, AIAA SciTech*, January 2016.

[30]Stevens, B. L. and Lewis, F. L., *Aircraft Control and Simulation*, Wiley-Interscience Publication, 2nd ed., 2003.

[31]de Visser, C. C., Mulder, J. A., and Chu, Q. P., "A Multidimensional Spline Based Global Nonlinear Aerodynamic Model for the Cessna Citation II," *AIAA Atmospheric Flight Mechanics Conference*, August 2010.

[32]Shah, G. H., "Aerodynamic Effects and Modeling of Damage to Transport Aircraft," *AIAA Atmospheric Flight Mechanics Conference and Exhibit*, August 2008.

[33]Bacon, B. J. and Gregory, I. M., "General Equations of Motion for a Damaged Asymmetric Aircraft," *AIAA Atmospheric Flight Mechanics Conference and Exhibit*, August 2007.

[34]Williams, J. E. and Vukelich, S. R., "The USAF Stability and Control Digital Datcom, Volume I, Users Manual," Technical Report AFFDL-TR-79-3032 (AD A086557), Flight Controls Division, Air Force Flight Dynamics Laboratory, Wright-Patterson Air Force Base, Ohio 45433, April 1979.

[35]Sadraey, M. H., *Aircraft Design: A Systems Engineering Approach*, Aerospace Series, John Wiley & Sons, 1st ed., October 2012.

[36]Finck, R. D., "USAF Stability and Control Datcom," Technical Report AFWAL-TR-83-3048, Flight Controls Division, Air Force Flight Dynamics Laboratory, Wright-Patterson Air Force Base, Ohio 45433, April 1978.

Part II

Introduction, Literature Review and Conclusion

Chapter 1

Introduction

A recent study by Commercial Aviation Safety Team (CAST)/International Civil Aviation Organization (ICAO) shows that the Loss of Control (LOC) in flight is the primary cause of fatal accidents in civil aviation. The study presents a statistical analysis of aircraft accidents during the period of 2002 till 2011 and it is indicated that the LOC comprise of as much as 23% of all the fatal aircraft accidents (Boeing, 2012). LOC entails that the aircraft has left the safe flight envelope, which is the set of safe flight conditions. In terms of flight performance, any damage to the aircraft or system failure degrades the flying qualities and hence require immediate attention to maintain the integrity of an aircraft (Lopez & Sarigul-Klijn, 2010). Because of the degraded flying qualities due to damage, the safe flight envelope may *shrink* and the aircraft may find itself outside of this changed safe flight envelope which leads to LOC, this is shown in Figure 1-1. Although the system dynamics may completely change as a result of a damage, these LOC related accidents can still be prevented using unconventional control strategies. A research is conducted by the Integrated Resilient Aircraft Control (IRAC) team at National Aeronautics and Space Administration (NASA) Aviation Safety Program that is focused on enhancing the flight control capabilities to prevent LOC and to safely land an aircraft (NASA Aviation Safety Program, 2009).

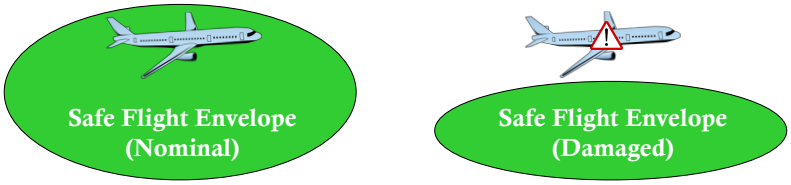

(a) Nominal Aircraft (b) Damaged Aircraft

Figure 1-1: Loss of Control due to Damage

In order to prevent the LOC, it is very important to have the knowledge about the restricted safe flight envelope of an impaired aircraft (T. J. J. Lombaerts, 2010; Stroosma, Smali, Lombaerts, & Mulder, 2008; T. Lombaerts et al., 2015) so that it can be made sure that the

aircraft does not leave the safe flight envelope. This information also increases pilot's overall situation awareness significantly (Stroosma et al., 2008; T. Lombaerts et al., 2015).

The flight envelope has been estimated in the literature by means of various methods. The estimation methods include wind tunnel testing, flight experiments and the model based computation of achievable trim points (Goman, Khramtsovsky, & Kolesnikov, 2008; Keller, McKillip, & Kim, 2009) or using a vortex lattice algorithm coupled with an extended kalman filter to estimate the performance flight envelope (Menon, Sengupta, Vaddi, Yang, & Kwan, 2013). However, a more extensive and detailed method is to estimate the safe flight envelope by considering it to be a non-linear reachability problem and to obtain the solution by numerically solving the Hamilton Jacobi Bellman (HJB) partial differential equations (PDE) or by Hamilton Jacobi Isaacs (HJI) PDE equations when the presence of disturbances are considered in the analysis. Reachability set analysis allows a very accurate estimation of the safe flight envelope of an aircraft, however, this approach is computationally expensive and the major challenge associated with such an analysis is the "curse of dimensionality".

At the present time there is very little knowledge of how different failures and damages affect the overall safe flight envelope of an aircraft. This information, however, is of extreme significance for a novel database approach to the real time flight envelope prediction and protection, that is currently being researched at the Control & Simulation (C&S) division of the Aerospace Faculty, Delft University of Technology (DUT). The basic principle of the database approach is that instead of trying to solve the HJI/HJB equations in real time, a database of safe flight envelopes corresponding to the most often occurring failures at various flight conditions is created offline. A quick classification of the failure is made when a failure is encountered during the flight, the database of safe flight envelopes is then accessed and interpolated to estimate the safe flight envelope. This estimated safe flight envelope is then used by the Flight Control Computer (FCC) to execute the flight envelope protection algorithm. Moreover, the estimated safe flight envelope is also conveyed to the pilot in order to improve the overall situation awareness. Figure 1-2 shows an overview of the database approach to flight envelope estimation and protection.

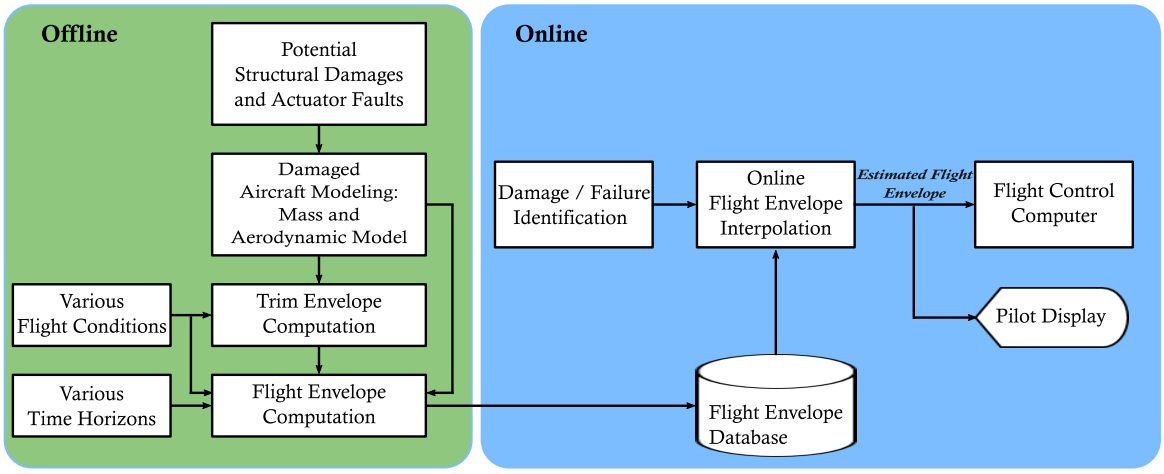

Figure 1-2: The Database Approach

1-1 Thesis Objectives and Research Questions

Focus of the current research is on the offline part of the database approach, in order to investigate the feasibility of the database approach. The main objective of this research is to construct a database of the safe flight envelopes corresponding to the most often occurring structural damages at various flight conditions. The framework of this research is optimal control and reachability analysis. The focus of the research expands to aerodynamic modeling of the damaged aircraft. The *research question* that is to be answered is:

"How do structural failures affect the safe flight envelope of an aircraft, and how can these effects be grouped into categories?".

The main research question has been sub-divided into following research questions based on different research areas that are related to the safe flight envelope estimation.

1. In addition to structural failures, how do different flight conditions and time horizons affect the safe flight envelope of an aircraft?
2. Is it possible to interpolate between the safe flight envelopes within the database?
3. How do different structural damages affect the aerodynamic model structure and the aerodynamic model parameters?
4. How can the principle of time scale separation be used in order to solve the higher dimensional reachability problem?

The research objective is achieved in the context of above mentioned research questions. The research areas that are explored in order to answer the defined research questions include: reachability set theory, optimal control formulation, level set method, time scale separation and modeling of the damaged aircraft.

1-2 Research Approach

The first step was to conduct a detailed literature review on various concepts related to the safe flight envelope estimation and modeling of the damaged aircraft. After completing the in-depth literature study, the physical and the aerodynamic model of the damaged aircraft was developed. The system, based on the flight dynamics and the aerodynamic model, was then analyzed for the feasibility of implementing the principle of time scale separation in order to compute the higher dimensional safe flight envelopes with better computational efficiency. Thereafter, the trim envelopes and then eventually the safe flight envelopes for Cessna Citation II were computed. The safe flight envelopes computed for various damages at different flight conditions were analyzed and the research questions outlined in Section 1-1 were answered in light of the research outcome.

1-3 Thesis Outline

This thesis report consists of three parts. Part I, presented earlier, contains the technical paper that delineate all the important concepts, methodologies, results and discussions on the results. Part II consist of three chapters, starting with the current chapter. Chapter 2 present a state-of-the-art literature survey in the field of reachability set theory, safe flight envelope estimation and damaged aircraft modeling. Conclusion on the current research and recommendations for the future research work, based on the results presented in the technical paper, are presented in Chapter 3. Lastly, Part III list all the appendices that contain additional results.

Chapter 2

Literature Review / State-of-the-Art

This chapter presents a detailed literature survey relevant to the current research. Various concepts related to the safe flight envelope estimation are discussed in the existing literature and researched thus far. In order to put things in perspective, different aspects related to the research are presented in the following structure: The safe flight envelope is formally defined in the first section. Section 2-2 provides a theoretical background on the subject of reachability set theory and explains its relevance to the safe flight envelope estimation. Section 2-3 presents a discussion on the challenge associated with the reachability set analysis i.e., "curse of dimensionality". Lastly, in section 2-4, an overview of the current research in the field of damaged aircraft modeling is presented.

2-1 The Safe Flight Envelope

Before we can elaborate upon the safe flight envelope estimation methods, it is necessary to give a formal definition of the safe flight envelope. The standard definition of the flight envelope refers to a region of airspeed and altitude where an aircraft is required to operate or a constrained area in the velocity versus load factor graph. These definitions can be found in any textbook on aircraft performance (Anderson, 1998; Ruijgrok, 2007). However, for the purpose of avoiding LOC, we are interested in the safe flight envelope which is formally defined as: (Oort, 2011)

The set of aircraft's state space for which the aircraft can be safely controlled and loss-of-control can easily be avoided.

This set is also referred to as the dynamic flight envelope (Oort, 2011) or the immediate flight envelope (Tang et al., 2009). Moreover, a distinction is made by (Tang et al., 2009) between the *immediate flight envelope* and the *extended flight envelope* which can be considered as the structural envelope and include the constraints like structural integrity. It is stated that the immediate flight envelope should be used for the flight envelope protection problem while the extended envelope is useful for broader functions such as path planning.

2-2 Reachability Set Theory

The reachability set theory is widely used in the safety analysis. Reachability set theory studies the behavior of set of trajectories that emerge from a dynamic system; that whether these trajectories can reach from one point to another in a given time.

Consider a continuous time system $\dot{\mathbf{x}} = \mathbf{f}(\mathbf{x}, \mathbf{u}, t)$, a time horizon $T \geq 0$, set of control inputs $\mathbf{u} \in U$ and a set of states K. There are three main sets that can be formulated associated with the set K and the trajectories that lead to K over a time horizon T (Lygeros, 2004).

Viability $\mathcal{V}(t, K)$: Set of all the states $\mathbf{x}(\cdot)$ for which there exist at least one input $\mathbf{u}(\cdot) \in U_{[0,T]}$ such that $\mathbf{x}(t) \in K$ for all $t \in [0, T]$.

Invariance $\mathcal{I}(t, K)$: Set of all the states $\mathbf{x}(\cdot)$ for which there exist all the inputs $\mathbf{u}(\cdot) \in U_{[0,T]}$ such that $\mathbf{x}(t) \in K$ for all $t \in [0, T]$.

Reachability $\mathcal{R}(t, K)$: Set of all the states $\mathbf{x}(\cdot)$ for which there exist at least one input $\mathbf{u}(\cdot) \in U_{[0,T]}$ and $t \in [0, T]$ such that $\mathbf{x}(t) \in K$.

By comparing the above sets, it can be stated that:

$$\mathcal{I}\left(t, K\right) \subset \mathcal{V}\left(t, K\right) \subset \mathcal{R}\left(t, K\right) \tag{2-1}$$

Moreover, the principle of duality relates the reachability and the invariant set as follows,

$$\mathcal{R}\left(t, K\right) = \left(\mathcal{I}\left(t, K^c\right)\right)^c \tag{2-2}$$

Figure 2-1 shows an illustration of these three sets. The smallest of these sets, as stated in Eq. 2-1, is the invariant set. It is the set of states where all the inputs lead to trajectories that remain inside the trim set K throughout the time horizon T. Next is the viability set, which is the largest subset of the trim set K. It can be seen that there are trajectories extending outside the trim set K, however, there is at least one input that is keeping the trajectory inside the trim set over the time horizon T. Lastly, the reachability set consists of all the states within and outside the trim set K for which at least one input $\mathbf{u}(\cdot)$ can bring the trajectory to the target set K within a time $t \in [0, T]$.

The system $\dot{\mathbf{x}} = \mathbf{f}(\mathbf{x}, \mathbf{u}, t)$ can be evolved forward and backwards in time, which can give us two further types of reachability set; forward and backward reachable sets:

Forward Reachable Set $\mathcal{R}_{\mathcal{F}}(t, K)$: Set of all the states $\mathbf{x}(\cdot)$ for which a control input $\mathbf{u}(\cdot) \in U_{[0,T]}$ exists at time $t \in [0, T]$, such that this set can be approached from at least one point in the trim envelope K.

Backward Reachable Set $\mathcal{R}_{\mathcal{B}}(t, K)$: Set of all the states $\mathbf{x}(\cdot)$ for which a control input $\mathbf{u}(\cdot) \in U_{[0,T]}$ exists at time $t \in [0, T]$, such that at least one state in the trim envelope K can be reached.

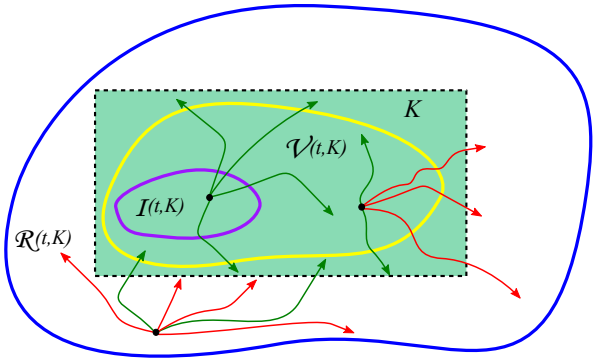

Figure 2-1: Viability (Yellow), Invariance (Magenta) and (backward) Reachability Set (Blue), Green: Successful trajectories; Red: Unsuccessful trajectories

2-2-1 Optimal Control Formulation

The *viability* and the *invariant* set, defined in the previous section, can be linked to SUPMIN and INFMIN optimal control problems respectively (Lygeros, 2004). Suppose that the open set K is associated with the zero level set of a function $l : \mathbb{R}^n \to \mathbb{R}$ by $K = \{\mathbf{x} \in \mathbb{R}^n \,|\, l(\mathbf{x}) > 0\}$, then the viability set can be given as:

$$\mathcal{V}(t,K) = \left\{ \mathbf{x} \in \mathbb{R}^n | V_1(\mathbf{x},t) = \sup_{\mathbf{u}(\cdot)\in U_{[t,T]}} \min_{\tau\in[t,T]} l\left(\phi\left(\tau,t,\mathbf{x},u(\cdot)\right)\right) > 0 \right\} \tag{2-3}$$

In the above equation $\phi(\tau,t,\mathbf{x},u(\cdot))$ is the state trajectory. Similarly, assume a closed set L that is associated with the level set of a continuous function $l : \mathbb{R}^n \to \mathbb{R}$ by $L = \{\mathbf{x} \in \mathbb{R}^n \,|\, l(\mathbf{x}) \geq 0\}$, then the invariant set can be given as:

$$\mathcal{I}(t,K) = \left\{ \mathbf{x} \in \mathbb{R}^n | V_2(\mathbf{x},t) = \inf_{\mathbf{u}(\cdot)\in U_{[t,T]}} \min_{\tau\in[t,T]} l\left(\phi\left(\tau,t,\mathbf{x},u(\cdot)\right)\right) \geq 0 \right\} \tag{2-4}$$

It is suggested by (Lygeros, 2004) that the characterization of value functions V_1 and V_2, given in Eqs. 2-3 and 2-4 respectively, can be represented as viscosity solutions to Hamilton-Jacobi partial differential equations. Hence, the viability set can be written in the form of HJB PDE as,

$$\frac{\partial V_1}{\partial t}(\mathbf{x},t) + \min_{\tau\in[t,T]} \left\{ 0, \sup_{\mathbf{u}(\cdot)\in \mathrm{U}_{[t,T]}} \frac{\partial V_1}{\partial \mathbf{x}}(\mathbf{x},t)\, \mathbf{f}(\mathbf{x},\mathbf{u},t) \right\} = 0 \tag{2-5}$$

And the invariant set is written in the form of HJB PDE as,

$$\frac{\partial V_2}{\partial t}(\mathbf{x},t) + \min_{\tau\in[t,T]} \left\{ 0, \inf_{\mathbf{u}(\cdot)\in \mathrm{U}_{[t,T]}} \frac{\partial V_2}{\partial \mathbf{x}}(\mathbf{x},t)\, \mathbf{f}(\mathbf{x},\mathbf{u},t) \right\} = 0 \tag{2-6}$$

The HJ PDE given by Eqs. 2-5 and 2-6 can be solved using the level set method either as an initial value problem or a terminal value problem in order to get a forward or a backward

set respectively. Moreover, the principle of duality as given by Eq. 2-2, is used to get the reachability set.

2-2-2 Safe Flight Envelope as a Reachability Set

Safe flight envelope estimation as a reachability set problem has been researched in the recent past(Oort, 2011; Lygeros, 2004, 2003; Oort, Chu, & Mulder, 2011), the same with uncertainty quantification and robustness in the estimated values of aerodynamic derivatives is also discussed in detail(Schuet, Lombaerts, Acosta, Wheeler, & Kaneshige, 2014; T. J. J. Lombaerts et al., 2013). The idea is to observe the dynamic behavior of the trim states as they evolve over a certain time horizon T i.e., reachability from the trim envelope (set of trim states). The trim envelope, which is the set of stable and controllable states, is considered as a-priori safe set. In terms of reachability set, the *safe flight envelope* is defined as the set of states that lie in the intersection of forward and backward reachable sets. The forward reachable set refers to the set of states to which an aircraft can easily maneuver from the stable trim set. On the other hand, the backward reachable set (or the survivable envelope (T. J. J. Lombaerts et al., 2013)) refers to the set of states from where an aircraft can recover back to the stable trim set. Hence, the safe set is the intersection between the aircraft's capability to maneuver from the trim set (forward reachable set) and the survivable capacity of an aircraft (backward reachable set). This is illustrated in Figure 2-2.

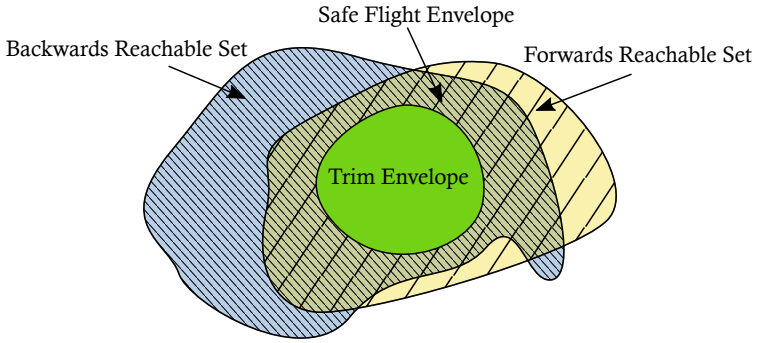

Figure 2-2: Safe Flight Envelope (Oort, 2011)

It is also very important to define an accurate trim set in order to obtain a correct reachability set. Any untrimmed state which is part of the initial set will lead to an inaccurate safe flight envelope. Computation of the trim states have been discussed in detail in the existing literature. A common approach to compute the trim set is to minimize a cost function using a numerical optimization routine (Marco, Duke, & Berndt, 2007; Yi & Atkins, 2010). The trim set can also be found through interval analysis (Kampen, Chu, Mulder, & Emden, 2007) and bifurcation and continuation methods (Ananthkrishnan & Sinha, 2001),

2-2-3 Level Set Method

In section 2-2-1, it was mentioned that the Eqs. 2-5 and 2-6 are solved numerically using the level set method in order to compute the reachability set. The level set method is briefly introduced in this section.

A particular set or an $n-$dimensional region can be represented either explicitly or by using an implicit function. Consider a closed region whose boundary is defined as *interface* i.e, the border between the inner and the outer part of the region. Now in the explicit representation, all the points that are part of the interface will be explicitly defined. However, in an implicit representation, the interface is defined as an isocontour of some function $\Phi(\mathbf{x}) = c$. Consider, for example, a unit circular region as shown in Figure 2-3, whose interface is *implicitly* defined by the $\Phi(\mathbf{x}) = c$ isocontour. The explicit representation of this interface will be a unit circle $\partial\Omega = \{\mathbf{x}| \, |\mathbf{x}| = 1\}$.

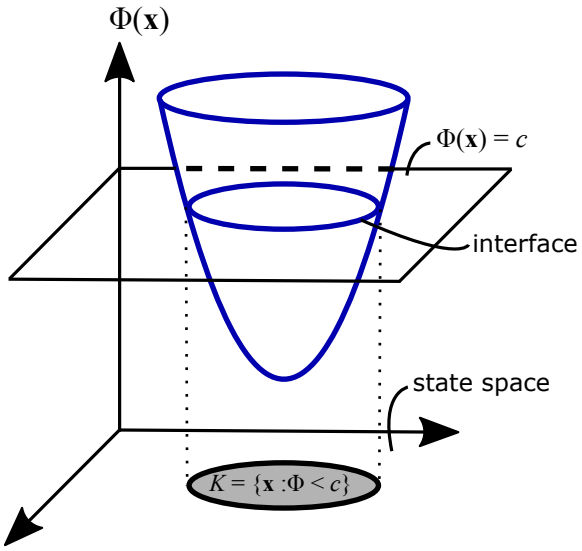

Figure 2-3: Implicit Representation of a Unit Circle

Level set method deals with the dynamic behavior of the implicitly defined surfaces. A detailed introduction on the topic of level set method is provided by (Osher & Fedkiw, 2003). In order to achieve a reachable set for defined initial or target set K, the interface has to be evolved in time. Suppose that the velocity of each point on the interface is given by $\mathbf{f}(\mathbf{x})$. Given this velocity field, every point on the surface can be evolved in time. This can be achieved by solving the ordinary differential equation (ODE) of the form,

$$\frac{d\mathbf{x}}{dt} = \mathbf{f}(\mathbf{x}) \tag{2-7}$$

This direct formulation of interface evolution equation is called *Lagrangian* formulation. However, it is argued by (Osher & Fedkiw, 2003) that the Lagrangian formulation is mesh-unstable and the accuracy of this method declines quickly due to deformation of the surface elements, unless the interface is regulated and smoothed on regular intervals.

In order to avoid such problems, it is suggested to use the implicit function $\Phi(\mathbf{x})$ to represent and evolve the interface. This is achieved by the following partial differential equation,

$$\Phi_t + \nabla\Phi.\mathbf{f}(\mathbf{x}) = 0 \tag{2-8}$$

where the first term refers to the partial derivative in the time variable t. Eq. 2-8 is the *Eulerian* formulation and is called the *level set equation*. It represents the motion of interface

where $\Phi(\mathbf{x}) = \mathbf{0}$. Level set equation as given in Eq. 2-8 is an example of Hamilton-Jacobi PDE of the form,

$$\Phi_t + H(\nabla\Phi) = 0 \tag{2-9}$$

Note that, Eq. 2-9 is identical to the HJ PDE given by Eqs. 2-5 and 2-6. Eqs. 2-5 and 2-6 are solved numerically using the level set toolbox, developed in MATLAB® at Stanford University (Mitchell & Tomlin, 2000; Mitchell, Bayen, & Tomlin, 2001), using the algorithm presented by (Osher & Fedkiw, 2003).

2-2-4 Implementation of Level Set Method

It was stated in the previous section that the Eqs. 2-5 and 2-6 are solved numerically using the level set toolbox, either as an initial value problem or a terminal value problem. There are various techniques that can be implemented in the toolbox that allow us to set up one standard problem for the forward reachable set, backward reachable set and the invariant or the viability set.

The relation between initial and terminal value problem for HJ equations is presented by (Melikyan, Akhmetzhanov, & Hovakimyan, 2007) as:

$$H^t(\mathbf{x}, \nabla_\mathbf{x}, t) = -H^i(\mathbf{x}, -\nabla_\mathbf{x}, t) \tag{2-10}$$

where H^t is the Hamiltonian for the terminal value problem and H^i is the Hamiltonian for the initial value problem. Firstly, the optimality conditions for choosing optimal inputs are *tricked* by using opposite gradients. Secondly, the temporal direction of integration is reversed. This is achieved by simply multiplying the Hamiltonian of initial value problem H^i with -1. Eq. 2-10 allow us to formulate the backward reachability problem as an initial value problem. Summary of the invariant and the viability set, both as initial value and terminal value problem, is given as follows:

$$\mathcal{I}_\mathcal{B} = \begin{cases} \mathcal{I}(t,K) = \{\mathbf{x}|\Phi(\mathbf{x},t) > c\} \\ \Phi(\mathbf{x},t_0) = -g(\mathbf{x}) \\ \mathbf{u}^* = \min\limits_{\mathbf{u}} \{\mathbf{f}(\mathbf{x},\mathbf{u},t).\nabla_\mathbf{x}\} \\ H_\mathcal{B} = \min\limits_{\tau} \{0, -\mathbf{f}(\mathbf{x},\mathbf{u}^*,t).\nabla_\mathbf{x}\} \\ D_t\Phi(\mathbf{x},t) \leq 0 \end{cases} = \begin{cases} \mathcal{I}(t,K) = \{\mathbf{x}|\Phi(\mathbf{x},t) < c\} \\ \Phi(\mathbf{x},t_0) = +g(\mathbf{x}) \\ \mathbf{u}^* = \min\limits_{\mathbf{u}} \{\mathbf{f}(\mathbf{x},\mathbf{u},t). - \nabla_\mathbf{x}\} \\ H_\mathcal{B} = \min\limits_{\tau} \{0, -\mathbf{f}(\mathbf{x},\mathbf{u}^*,t).\nabla_\mathbf{x}\} \\ D_t\Phi(\mathbf{x},t) \geq 0 \end{cases}$$

$$\mathcal{I}_\mathcal{F} = \begin{cases} \mathcal{I}(t,K) = \{\mathbf{x}|\Phi(\mathbf{x},t) > c\} \\ \Phi(\mathbf{x},t_0) = -g(\mathbf{x}) \\ \mathbf{u}^* = \min\limits_{\mathbf{u}} \{\mathbf{f}(\mathbf{x},\mathbf{u},t). - \nabla_\mathbf{x}\} \\ H_\mathcal{F} = \min\limits_{\tau} \{0, \mathbf{f}(\mathbf{x},\mathbf{u}^*,t).\nabla_\mathbf{x}\} \\ D_t\Phi(\mathbf{x},t) \leq 0 \end{cases} = \begin{cases} \mathcal{I}(t,K) = \{\mathbf{x}|\Phi(\mathbf{x},t) < c\} \\ \Phi(\mathbf{x},t_0) = +g(\mathbf{x}) \\ \mathbf{u}^* = \min\limits_{\mathbf{u}} \{\mathbf{f}(\mathbf{x},\mathbf{u},t).\nabla_\mathbf{x}\} \\ H_\mathcal{F} = \min\limits_{\tau} \{0, \mathbf{f}(\mathbf{x},\mathbf{u}^*,t).\nabla_\mathbf{x}\} \\ D_t\Phi(\mathbf{x},t) \geq 0 \end{cases}$$

$$\mathcal{V}_{\mathcal{B}} = \begin{cases} \mathcal{V}(t,K) = \{\mathbf{x}|\Phi(\mathbf{x},t) > c\} \\ \Phi(\mathbf{x},t_0) = -g(\mathbf{x}) \\ \mathbf{u}^* = \max\limits_{\mathbf{u}} \{\mathbf{f}(\mathbf{x},\mathbf{u},t).\nabla_{\mathbf{x}}\} \\ H_{\mathcal{B}} = \min\limits_{\tau} \{0, -\mathbf{f}(\mathbf{x},\mathbf{u}^*,t).\nabla_{\mathbf{x}}\} \\ D_t\Phi(\mathbf{x},t) \leq 0 \end{cases} = \begin{cases} \mathcal{V}(t,K) = \{\mathbf{x}|\Phi(\mathbf{x},t) < c\} \\ \Phi(\mathbf{x},t_0) = +g(\mathbf{x}) \\ \mathbf{u}^* = \max\limits_{\mathbf{u}} \{\mathbf{f}(\mathbf{x},\mathbf{u},t). - \nabla_{\mathbf{x}}\} \\ H_{\mathcal{B}} = \min\limits_{\tau} \{0, -\mathbf{f}(\mathbf{x},\mathbf{u}^*,t).\nabla_{\mathbf{x}}\} \\ D_t\Phi(\mathbf{x},t) \geq 0 \end{cases}$$

$$\mathcal{V}_{\mathcal{F}} = \begin{cases} \mathcal{V}(t,K) = \{\mathbf{x}|\Phi(\mathbf{x},t) > c\} \\ \Phi(\mathbf{x},t_0) = -g(\mathbf{x}) \\ \mathbf{u}^* = \max\limits_{\mathbf{u}} \{\mathbf{f}(\mathbf{x},\mathbf{u},t). - \nabla_{\mathbf{x}}\} \\ H_{\mathcal{F}} = \min\limits_{\tau} \{0, \mathbf{f}(\mathbf{x},\mathbf{u}^*,t).\nabla_{\mathbf{x}}\} \\ D_t\Phi(\mathbf{x},t) \leq 0 \end{cases} = \begin{cases} \mathcal{V}(t,K) = \{\mathbf{x}|\Phi(\mathbf{x},t) < c\} \\ \Phi(\mathbf{x},t_0) = +g(\mathbf{x}) \\ \mathbf{u}^* = \max\limits_{\mathbf{u}} \{\mathbf{f}(\mathbf{x},\mathbf{u},t).\nabla_{\mathbf{x}}\} \\ H_{\mathcal{F}} = \min\limits_{\tau} \{0, \mathbf{f}(\mathbf{x},\mathbf{u}^*,t).\nabla_{\mathbf{x}}\} \\ D_t\Phi(\mathbf{x},t) \geq 0 \end{cases}$$

$\Phi(\mathbf{x},t)$ in the above equations is the viscous approximation of the value function and $g(\mathbf{x})$ is the terminal cost function or in our case it represents the trim set K. The forward and the backward reachability set can be obtained by applying the principle of duality as given by Eq. 2-2, on the forward and the backward invariant set respectively.

2-3 Curse of Dimensionality

Estimating the safe flight envelope as a reachability set using the level set method is computationally expensive; the time and the memory required grows significantly with the dimension of the problem. The computational complexity of the level set method is of the order $\mathcal{O}\left(N^{n+1}\right)$, with N being the number of computational grid points and n the dimension of the problem (Stapel, Visser, Chu, & Kampen, 2016). It has been suggested by (Kitsios & Lygeros, 2005) that the *"curse of dimensionality"* in the reachability analysis can be solved by exploiting the structure of the system dynamics using the principle of time scale separation and solving the reachability problem in a sequential manner; first for the faster dynamics and then for the slower dynamics.

Figure 2-4 shows the structure of time scale separation implemented for reachability computation by (Kitsios & Lygeros, 2005). First, the range of pseudo-controls (V, γ) is computed by defining the reachability problem for faster dynamics. In the next step, the viability set for the states with slower dynamics (x, y, h, ψ) has been estimated using the pseudo-controls (V, γ) and the actual optimal inputs (C_L, ϕ). This allows solving the higher dimensional reachability problem in two steps of lower dimensional reachability problems (two and four respectively). However, although the dynamics has been split into faster and slower dynamics, these six states belong to the low bandwidth dynamics and are slower than the states belonging to high bandwidth (faster) dynamics such as body angular rates and aerodynamic angles. The states belonging to fast dynamics will be of interest in case of a structural failure to the aircraft. Moreover, the reachability computation performed by Kitsios and Lygeros do not consider actual control inputs to the system rather *"virtual inputs"* in the form of lift coefficient C_L and roll angle ϕ.

(T. J. J. Lombaerts et al., 2013) has suggested a structure that incorporates faster dynamics and include actual aircraft control inputs for the reachability computation. This decomposition of aircraft dynamics based on the principle of time scale separation is presented in

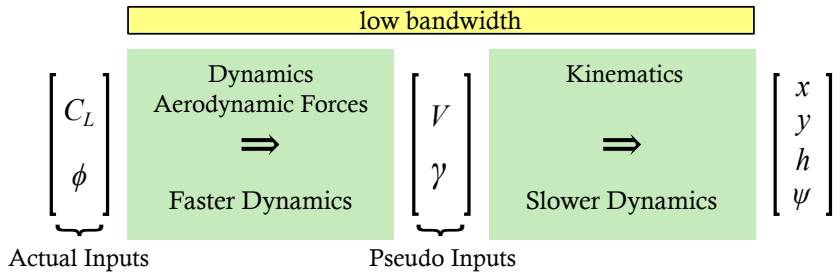

Figure 2-4: Time Scale Separation implemented by (Kitsios & Lygeros, 2005)

Figure 2-5. However, the sequence of reachability computation for faster dynamics suggested here is not feasible when only considering the control surface deflections as inputs for the reachability analysis. Consider nine-dimensional equations of motion of an aircraft (Stevens & Lewis, 2003). Firstly, the moment equations of motion in body-fixed reference frame are given by,

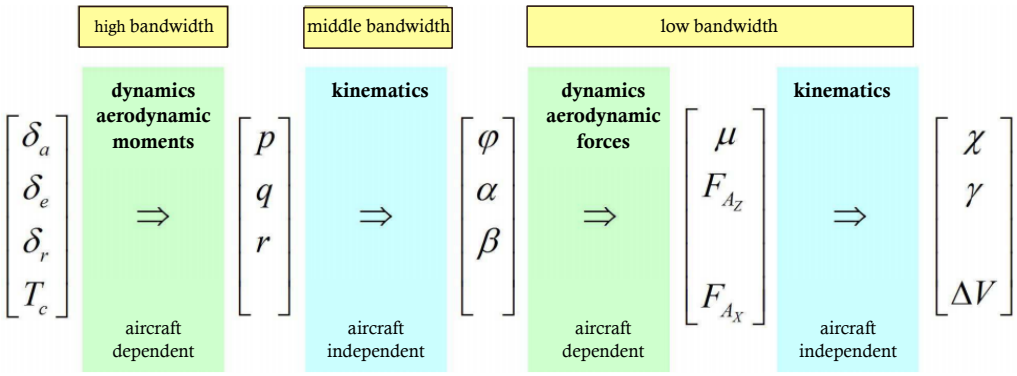

Figure 2-5: Time Scale Separation of Aircraft Dynamics (T. J. J. Lombaerts et al., 2013)

$$\begin{cases} \dot{p} = (c_1 r + c_2 p)\, q + c_3 \frac{1}{2}\rho V^2 SbC_l\left(\alpha, \beta, p, r, \delta_a, \delta_r\right) + c_4 \frac{1}{2}\rho V^2 SbC_n\left(\alpha, \beta, p, r, \delta_a, \delta_r\right) \\ \dot{q} = c_5 pr - c_6\left(p^2 - r^2\right) + c_7 \frac{1}{2}\rho V^2 S\bar{c}C_m\left(\alpha, q, \delta_e\right) \\ \dot{r} = (c_8 p - c_2 r)\, q + c_4 \frac{1}{2}\rho V^2 SbC_l\left(\alpha, \beta, p, r, \delta_a, \delta_r\right) + c_9 \frac{1}{2}\rho V^2 SbC_n\left(\alpha, \beta, p, r, \delta_a, \delta_r\right) \end{cases} \tag{2-11}$$

where the moments of inertia are defined as, with $\Gamma = J_{xx}J_{zz} - J_{zx}^2$,

$$\Gamma c_1 = \left(J_{yy} - J_{zz}\right) J_{zz} - J_{zx}^2 \qquad \Gamma c_4 = J_{zx} \qquad c_7 = \frac{1}{J_{yy}}$$

$$\Gamma c_2 = \left(J_{xx} - J_{yy} + J_{zz}\right) J_{zx} \qquad c_5 = \frac{J_{zz} - J_{xx}}{J_{yy}} \qquad \Gamma c_8 = \left(J_{xx} - J_{yy}\right) J_{xx} + J_{zx}^2$$

$$\Gamma c_3 = J_{zz} \qquad c_6 = \frac{J_{zx}}{J_{yy}} \qquad \Gamma c_9 = J_{xx}$$

Secondly, the force equations of motion in the wind-axes reference frame are,

$$\begin{cases} \dot{V} = \dfrac{1}{m}\left(T\cos\alpha\cos\beta - \frac{1}{2}\rho V^2 S C_D(\alpha) + mg_1\right) \\ \dot{\beta} = p\sin\alpha - r\cos\alpha + \dfrac{1}{mV}\left[-T\cos\alpha\sin\beta + \frac{1}{2}\rho V^2 S C_Y(\alpha,\beta,p,\delta_r) + mg_2\right] \\ \dot{\alpha} = q - p\cos\alpha\tan\beta - r\sin\alpha\tan\beta + \dfrac{1}{mV\cos\beta}\left[-T\sin\alpha - \frac{1}{2}\rho V^2 S C_L(\alpha,q,\delta_f) + mg_3\right] \end{cases} \tag{2-12}$$

where the components of the gravity vector in wind-axes are given by,

$$\begin{aligned} g_1 &= g\left(-\cos\alpha\cos\beta\sin\theta + \sin\beta\sin\phi\cos\theta + \sin\alpha\cos\beta\cos\phi\cos\theta\right) \\ g_2 &= g\left(\cos\alpha\sin\beta\sin\theta + \cos\beta\sin\phi\cos\theta - \sin\alpha\sin\beta\cos\phi\cos\theta\right) \\ g_3 &= g\left(\sin\alpha\sin\theta + \cos\alpha\cos\phi\cos\theta\right) \end{aligned}$$

And lastly, the kinematic equations are written as,

$$\begin{cases} \dot{\phi} = p + \tan\theta\left(q\sin\phi + r\cos\phi\right) \\ \dot{\theta} = q\cos\phi - r\sin\phi \\ \dot{\psi} = q\frac{\sin\phi}{\cos\theta} + r\frac{\cos\phi}{\cos\theta} \end{cases} \tag{2-13}$$

From Eqs. 2-11 and 2-12, it can be seen that the p, q, r and V, β, α are dependent upon each other. The safe flight envelope for angular rates (p, q, r) cannot directly be obtained using the reachability computation without the information about the bounds of velocity V, sideslip angle β and angle of attack α; yet the safe flight envelope for V, β and α is computed at the later stage according to this structure, see Figure 2-5. Similarly, in order to obtain the safe flight envelope for V, β and α, we need the information about the safe flight envelope for Euler angles (ϕ, θ, ψ) and in order to compute the safe flight envelope for Euler angles, we again require the information of angular rates, see Eq. 2-13. It can be concluded, that although the principle of time scale separation is useful for the slow dynamics as suggested by (Kitsios & Lygeros, 2005), it is not feasible and possible to use the same principle of time scale separation for the fast dynamics. All in all, a nine-dimensional reachability problem has to be solved which is not feasible with the current computational potential.

Estimation of the safe flight envelope in a reachability framework using the actual aircraft control inputs (stabilizer deflection and engine thrust) has only been discussed once (Oort et al., 2011; Oort, 2011). Apart from that, in the literature hitherto (T. J. J. Lombaerts et al., 2013; T. Lombaerts et al., 2015; Tang et al., 2009; Lygeros, 2004; Schuet et al., 2014; Kitsios & Lygeros, 2005), reachability computation has only been performed for the slower dynamics and therefore the angle of attack and the sideslip angle etc. have been used as the "*virtual inputs*". However, the changes in the safe flight envelope of these virtual inputs due to a structural damage or a system failure is not considered.

2-4 Modeling of the Damaged Aircraft

Solving the reachability problem using the level set method rely on the physical model as indicated by the term $\mathbf{f}(\mathbf{x}, \mathbf{u}, t)$ in Eqs. 2-5 and 2-6. Hence, in order to estimate the safe flight envelope, it is essential to have a dynamic model of an aircraft. One of the key parts of such a dynamic model is the aerodynamic model. These aerodynamic models can either be simple polynomial models or more complex multivariate spline models (Visser, Mulder, & Chu, 2010). In case of a structural damage to an aircraft the aerodynamic model parameters, in addition to mass and inertial properties of the aircraft, will change. Furthermore, changes in the model structure may also arise due to inertial couplings. The additional parameters that may appear in the model structure of an asymmetrically damaged aircraft can be estimated either by wind tunnel testing or by a Computational Fluid Dynamics (CFD) analysis. A detailed wind tunnel research was conducted at the NASA Langley Research Center in order to study the effects on the aerodynamic model parameters (such as pitching moment coefficient C_m, rolling moment coefficient C_l etc.) of different damage case scenarios to a conventional transport aircraft (Shah, 2008). Moreover, (Bacon & Gregory, 2007) from NASA Langley Research Center have presented a set of flight dynamics equations of motion for an asymmetrically damaged aircraft.

In the following paragraphs, we shall present the changes in the aerodynamic model structure due to structural damages presented in Table 2-1. Aerodynamic model structure changes are based on the results presented by (Shah, 2008) and underlying aircraft dynamics.

Table 2-1: Structural Damages investigated by (Shah, 2008)

Damage Type	Damage Subtype
Asymmetric Wing Damage	Spanwise Holes in wing
Asymmetric Horizontal Tail Damage	Spanwise Holes in horizontal tail
Vertical Tail Damage	Spanwise Holes in vertical tail

1. *Nominal Aircraft Model Structure*: Before we can discuss about the changes in the aerodynamic model, we need to define an aerodynamic model for the nominal aircraft. A simple polynomial aerodynamic model is considered and is presented as follows:

$$Longitudinal \begin{cases} C_X = C_{X_0} + C_{X_\alpha}\alpha + C_{X_q}\frac{q\bar{c}}{2V} + C_{X_{\delta_e}}\delta_e \\ C_Z = C_{Z_0} + C_{Z_\alpha}\alpha + C_{Z_q}\frac{q\bar{c}}{2V} + C_{Z_{\delta_e}}\delta_e \\ C_m = C_{m_0} + C_{m_\alpha}\alpha + C_{m_q}\frac{q\bar{c}}{2V} + C_{m_{\delta_e}}\delta_e \end{cases} \tag{2-14}$$

$$Lateral \begin{cases} C_Y = C_{Y_0} + C_{Y_\beta}\beta + C_{Y_p}\frac{pb}{2V} + C_{Y_r}\frac{rb}{2V} + C_{Y_{\delta_a}}\delta_a + C_{Y_{\delta_r}}\delta_r \\ C_l = C_{l_0} + C_{l_\beta}\beta + C_{l_p}\frac{pb}{2V} + C_{l_r}\frac{rb}{2V} + C_{l_{\delta_a}}\delta_a + C_{l_{\delta_r}}\delta_r \\ C_n = C_{n_0} + C_{n_\beta}\beta + C_{n_p}\frac{pb}{2V} + C_{n_r}\frac{rb}{2V} + C_{n_{\delta_a}}\delta_a + C_{n_{\delta_r}}\delta_r \end{cases} \tag{2-15}$$

2. *Damaged Aircraft Model Structure*:

   (a) Asymmetric Wing Damage: Because of the asymmetric nature of the damage, longitudinal aerodynamics will be affected by sideslip angle. Hence, the longitudinal model of the aircraft with asymmetric wing damage will be,

$$\begin{aligned} C_{X_{\text{damaged}}} &= C_{X_{\text{nominal}}} + \boxed{C_{X_\beta}\beta} \\ C_{Z_{\text{damaged}}} &= C_{Z_{\text{nominal}}} + \boxed{C_{Z_\beta}\beta} \\ C_{m_{\text{damaged}}} &= C_{m_{\text{nominal}}} + \boxed{C_{m_\beta}\beta} \end{aligned} \tag{2-16}$$

   Moreover, damage to one wing of the aircraft will result in an asymmetric lift. This will have two consequences in the lateral aerodynamic model structure:

   - Roll damping may not be symmetric anymore i.e., roll damping with positive and negative roll rate will not be same.
   - There will be an additional influence from angle of attack and pitch rate.

$$\begin{aligned} C_{Y_{\text{damaged}}} &= C_{Y_{\text{nominal}}} + \boxed{C_{Y_\alpha}\alpha + C_{Y_q}\frac{q\bar{c}}{2V}} \\ C_{n_{\text{damaged}}} &= C_{n_{\text{nominal}}} + \boxed{C_{n_\alpha}\alpha + C_{n_q}\frac{q\bar{c}}{2V}} \\ C_{l_{\text{damaged}}} &= C_{l_0} + C_{l_\beta}\beta + C_{l_r}\tfrac{rb}{2V} + C_{l_{\delta_a}}\delta_a + C_{l_{\delta_r}}\delta_r + \boxed{C_{l_{p^+}}\frac{p^+b}{2V} + C_{l_{p^-}}\frac{p^-b}{2V} + C_{l_\alpha}\alpha + C_{l_q}\frac{q\bar{c}}{2V}} \end{aligned} \tag{2-17}$$

   In the above equations, terms inside the box are additional terms that may appear due to the damage. The subscript *nominal* refers to the fact that the model structure is same as the model of the nominal aircraft but the model parameters may not be same. Also p^+ is positive roll rate and p^- is negative roll rate.

   (b) Asymmetric Horizontal Tail Damage: The only change is expected in the lateral aerodynamic model, where due to asymmetry the aerodynamic moments and force will additionally vary with angle of attack, pitch rate and elevator deflection.

$$\begin{aligned} C_{Y_{\text{damaged}}} &= C_{Y_{\text{nominal}}} + \boxed{C_{Y_\alpha}\alpha + C_{Y_q}\frac{q\bar{c}}{2V} + C_{Y_{\delta_e}}\delta_e} \\ C_{n_{\text{damaged}}} &= C_{n_{\text{nominal}}} + \boxed{C_{n_\alpha}\alpha + C_{n_q}\frac{q\bar{c}}{2V} + C_{n_{\delta_e}}\delta_e} \\ C_{l_{\text{damaged}}} &= C_{l_{\text{nominal}}} + \boxed{C_{l_\alpha}\alpha + C_{l_q}\frac{q\bar{c}}{2V} + C_{l_{\delta_e}}\delta_e} \end{aligned} \tag{2-18}$$

   No additional terms are expected in the longitudinal aerodynamic model. Only the aerodynamic model parameters will change.

   (c) Vertical Tail Damage: Because of the symmetry, no change in the model structure is expected in case of a vertical tail damage. There will be no control effectiveness in case of the complete vertical tail loss i.e., $C_{n_{\delta_r}} = C_{l_{\delta_r}} = 0$.

Chapter 3

Conclusions and Recommendations

The increase in the frequency of loss of control (LOC) related accidents in the civil aviation has sparked a strong world-wide interest in the efficient methods for online flight envelope prediction and protection. However, the safe flight envelope estimation is computationally expensive and hence, real time flight envelope prediction and protection is not feasible at this point in time. This is where the novel database approach, presented by (Tang et al., 2009) and reintroduced by (Zhang, Visser, & Chu, 2016a, 2016b), aims to provide the solution. The proposed approach uses a database to store the safe flight envelopes, computed offline, for "standard" structural failures at various flight conditions. In case of a structural damage or a system failure, this database of safe flight envelopes is then accessed and interpolated to estimate the safe flight envelope for the damaged aircraft. The database approach is based on the premise that the safe flight envelopes for an aircraft can be interpolated between various flight conditions, structural damages, system failures or time horizons etc.

This research was conducted in order to corroborate the above mentioned premise and to investigate the feasibility of the database approach towards online flight envelope prediction and protection. The research question was formulated as: *How do structural failures affect the safe flight envelope of an aircraft, and how can these effects be grouped into categories?*

In order to answer the research question, a three dimensional longitudinal safe flight envelope $(\alpha - \theta - q)$ with $\dot{V} = 0$ and a two dimensional lateral safe flight envelope $(\beta - r)$ with $\dot{p} = p = \dot{\phi} = \phi = 0$, for the nominal and the damaged Cessna Citation II was computed at various flight conditions and with different time horizons. For the purpose of decoupling the flight dynamics, only symmetrical damages with spanwise vertical tail damage were considered.

Nonlinear reachability set theory has been used as the framework to estimate the safe flight envelope. Level set method through an optimal control formulation, was employed to compute the reachable set and hence the safe flight envelope. Nonlinear reachability analysis require a physical model of an aircraft. Therefore, a straightforward method to estimate the physical parameters of the aircraft, was presented. Furthermore, the aerodynamic stability and control derivatives were estimated using Digital Datcom.

In light of the research questions and the results obtained during the course of this research, following conclusions are made:

- The size of the lateral safe flight envelope shrinks almost quadratically with spanwise vertical tail damage. Moreover, the longitudinal safe flight envelope remains same with the spanwise vertical tail damage. However, it shrinks drastically and almost vanishes with 100% tail loss. It can be concluded, that different structural damages affect the safe flight envelope differently, however, each damage type has a unique but consistent effect on the safe flight envelope that can be interpolated.
- Flight conditions i.e., different Mach numbers and altitudes, have almost linear effect on the safe flight envelope of Cessna Citation II; the safe flight envelope expands linearly with the increasing Mach and shrinks linearly with the increasing altitude. Similarly, the time horizon has also the same linear affect on the safe flight envelope of Cessna Citation II, and the safe flight envelope expands linearly with the increasing time horizon.
- The effects of various structural damages, investigated by (Shah, 2008), on the aerodynamic model structure were presented in section 2-4. It was suggested, that in case of an unsymmetrical damage, additional model parameters may appear in the aerodynamic model, based on the underlying flight dynamics.
- It was argued that the knowledge of states belonging to fast dynamics (i.e., safe flight envelope of fast dynamics) is very essential in case of a structural damage. However, in the literature, reachability computation has only been performed for slower dynamics, except once by (Oort et al., 2011; Oort, 2011).
- It was further demonstrated, that the principle of time scale separation is very useful for solving the problem of "curse of dimensionality" in the reachability analysis for the slower dynamics. However, the principle of time scale separation cannot be implemented for the faster dynamics in the reachability analysis, when only considering the aircraft control surfaces as inputs.

Based on the conclusions, that are derived from the current research, it can be argued that the database approach show promise towards online safe flight envelope estimation and protection. Furthermore, the current thesis laid the stepping stone for further research into the database approach towards flight envelope prediction and protection. Following are the recommendations, proposed for the future work:

- From the computed safe flight envelopes, it was observed that the reachability set extends far from the region, where the linear aerodynamic model and structural limits are valid. Therefore, these limits can be introduced in the reachability analysis which will assist in restricting the computational domain to a region of interest.
- In order to create an extensive database of safe flight envelopes, further research must consider the asymmetrical damages.
- The safe flight envelopes in the current research were computed without the consideration of external disturbances. For a more realistic safe flight envelope, further research must take into account atmospheric disturbances.
- Modeling of the damaged aircraft is an area of key importance for computing the accurate safe flight envelopes. Therefore, an extensive study must be conducted in the damaged aircraft modeling.

- In case of asymmetrical damages, the decomposition of flight dynamics into longitudinal and lateral dynamics will be no more valid. And a nine dimensional safe flight envelope for the fast dynamics will have to be computed. In order to compute, such a high dimensional safe flight envelope, efficient computational methods must be explored.

- The computed safe flight envelopes for Cessna Citation II were verified by performing the Monte Carlo simulations. An interesting fact was revealed by the Monte Carlo simulations, that the reachability set computes the safe flight envelope that is "theoretically" reachable, however, practically it might not be possible to reach such a state. This is due to the fact, that reachability analysis attempts to reach a particular state using "optimal control", but in real world, it might not be possible to mimic such an optimal control input for certain states.

  Therefore, it is proposed to investigate the feasibility of using Monte Carlo simulations for computing the safe flight envelopes. In the Monte Carlo simulation, a restriction can be imposed on the control inputs, such that the reachability set is composed of only those state trajectories that are feasible. This will result in a restricted, but practical safe flight envelope. Moreover, since the Monte Carlo simulation does not involve solving a HJI/HJB PDE at each grid point, it is postulated that it will be computationally efficient, when compared with the reachability analysis.

Part III

Appendices

Appendix A

Aerodynamic Derivatives Estimated by Digital Datcom

Aerodynamic effects of the structural damages were estimated using USAF Digital Datcom (Williams & Vukelich, 1979). Digital Datcom estimates the derivatives of symmetrical aircraft using the methods contained in the USAF Stability and Control Datcom (Data Compendium) (Finck, 1978). Digital Datcom allows the estimation of static stability, control device and the dynamic derivative characteristics of various symmetrical configurations at different flight conditions. Digital Datcom is developed on a modular basis and the modules represent the primary building blocks. Aircraft geometry and the flight conditions are coded using a standard editor through a series of NAMELIST statements.

The output of Digital Datcom is difficult to interpret as it presents the stability derivatives as an unstructured text file. A function `datcomimport()` is available in MATLAB® which takes the output file of Digital Datcom and import all the aerodynamic data into a cell array of structures.

Figures A-1 show the static stability derivatives obtained from Digital Datcom. First two plots show the lift coefficient and the drag coefficient variation with angle of attack. It can be seen that there is no significant change for nominal and the damaged aircraft. However, there is a small drop in the drag polar (decrease in drag) for complete tail loss. Third plot shows the C_{m_α} variation with the angle of attack. There is an improvement in the static longitudinal stability with the loss of vertical tail, but as soon as complete tail is lost the aircraft becomes longitudinally unstable. Improvement in the static longitudinal stability with spanwise loss in the vertical tail is due to the fact that the center of gravity is moving forward because of this loss and hence making the aircraft longitudinally stable. Fourth plot shows the variation of dihedral effect with the angle of attack. The slope decreases with the damage. Last two plots show the variation of yawing moment coefficient and side force coefficient with the sideslip angle. With 50% loss in the vertical tail, aircraft is already directionally unstable which can be seen by the negative slope C_{n_β}. Moreover, with the loss in vertical tail, the sideslip is generating less side force compared to the force generated for the nominal aircraft.

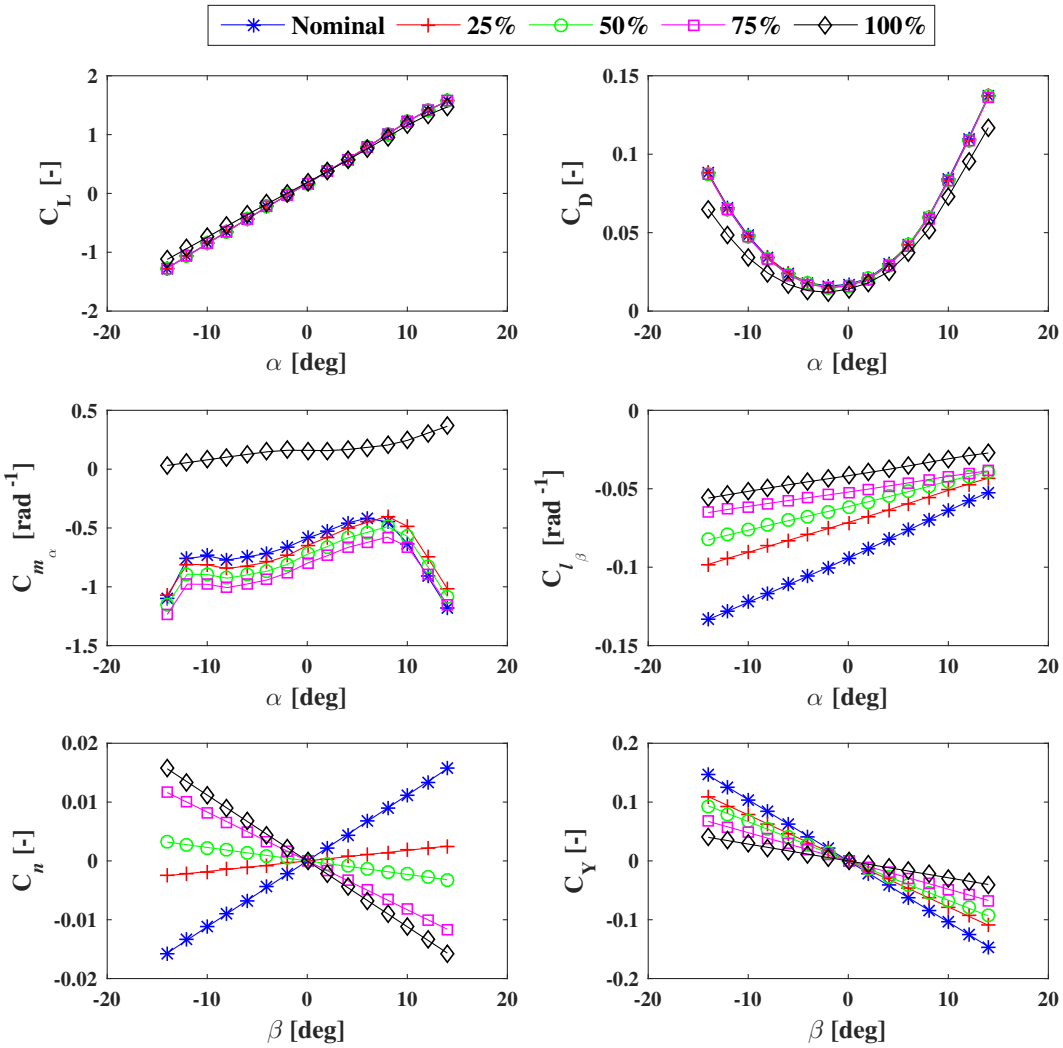

Figure A-1: Static Stability Derivatives (Sea Level, Mach = 0.4)

The dynamic stability derivatives are shown in Figure A-2. There is not much difference for most of the dynamic stability derivatives between the nominal and the damaged aircraft. However, there is a mark change in the yaw damping variation and has a similar degrading effect as the static characteristics shown by Cl_β plot in Figure A-1.

Lastly, Figure A-3 shows the variation of control derivatives of the aricraft. The symmetrical damage investigated in the current research, does not have a significant effect on the control derivatives. In the last two plots there is no curve shown for 100% tail loss which is obvious, because with the complete tail loss (hence the horizontal tail), there will be no elevator control effectiveness.

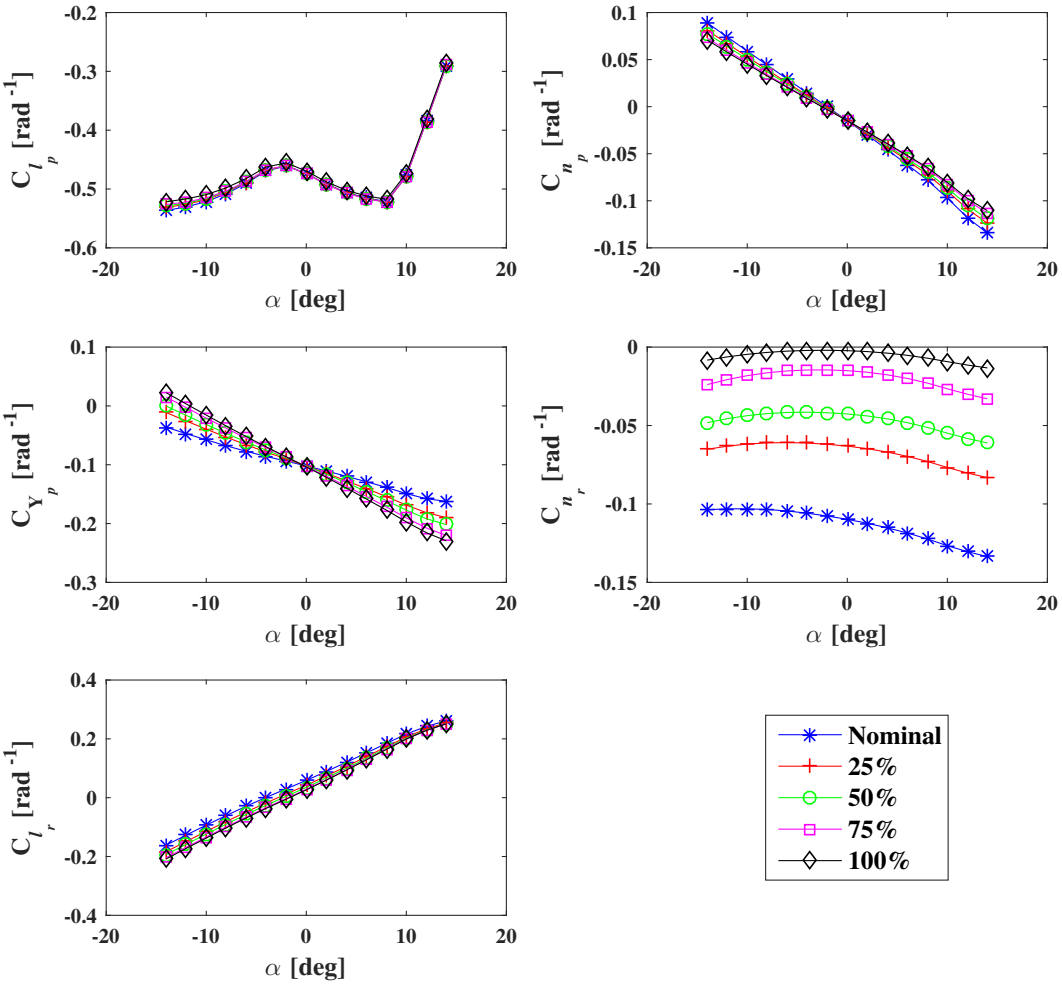

Figure A-2: Dynamic Stability Derivatives (Sea Level, Mach = 0.4)

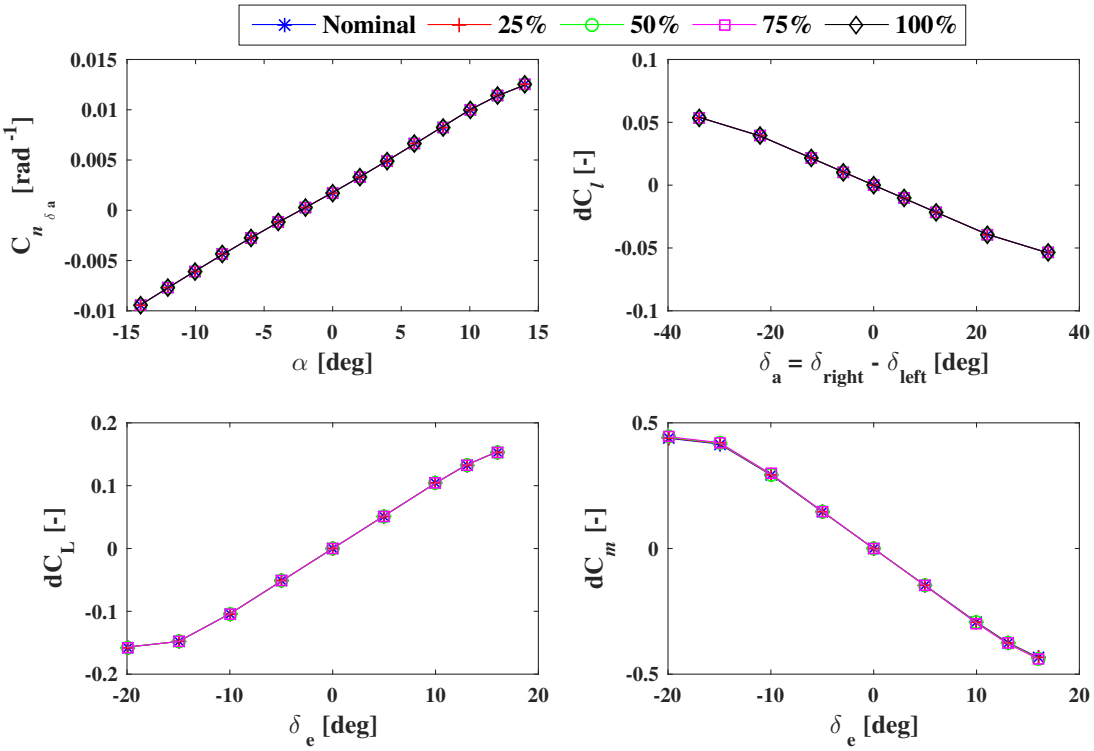

Figure A-3: Control Derivatives (Sea Level, Mach = 0.4)

Appendix B

Additional Safe Flight Envelopes

The safe flight envelopes that were computed in order to verify the interpolatibility within the database approach, are presented in this Appendix.

Figure B-1 presents the safe flight envelope for damaged Cessna Citation II with 40% and 60% vertical tail loss at Mach 0.4 and sea level.

Figure B-2(a) shows the safe flight envelope for nominal Cessna Citation II at Mach 0.35 and sea level. Whereas, the safe flight envelope for nominal Cessna Citation II at Mach 0.4 and sea level is shown in Figure B-2(b).

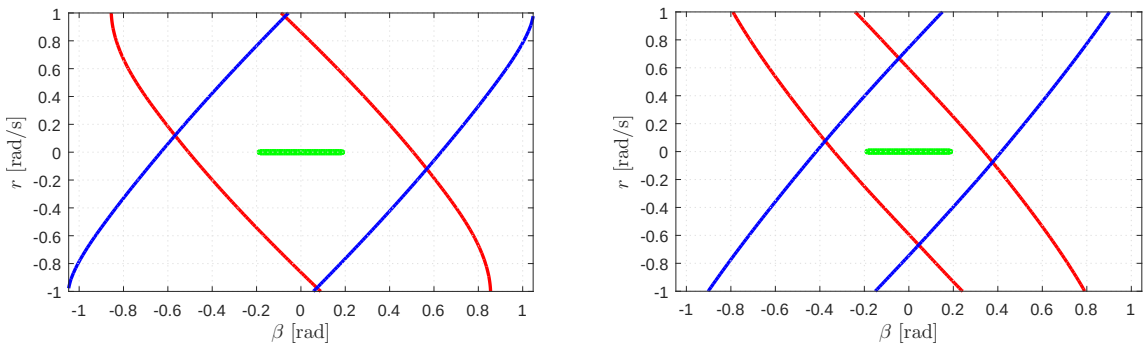

(a) 40% VT Loss

(b) 60% VT Loss

Figure B-1: Lateral Safe Flight Envelope for Damaged Cessna Citation II with $T = 1$ s at Mach 0.4, Sea Level, Green: Trim Envelope, Blue: Backward Reachable Set, Red: Forward Reachable Set

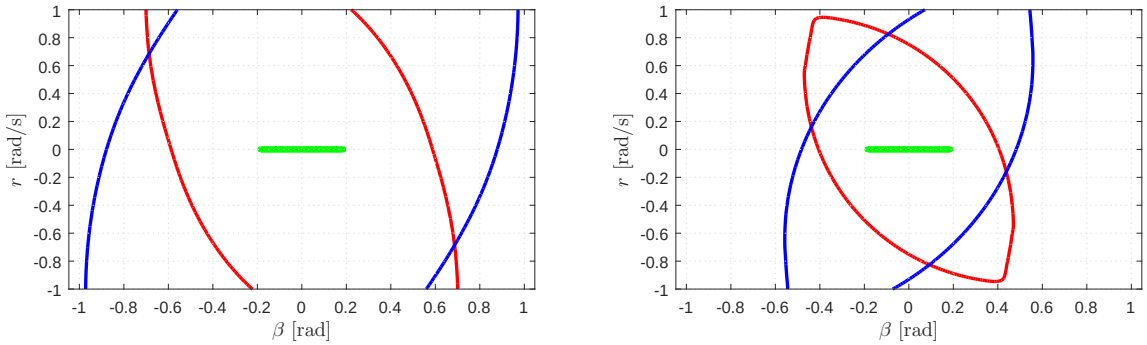

(a) Mach 0.35, Sea Level

(b) Mach 0.4, 7,500 m

Figure B-2: Lateral Safe Flight Envelope for Nominal Cessna Citation II with $T = 1$ s, Green: Trim Envelope, Blue: Backward Reachable Set, Red: Forward Reachable Set

References

Ananthkrishnan, N., & Sinha, N. K. (2001). Level Flight Trim and Stability Analysis using Extended Bifurcation and Continuation Procedure. *Journal of Guidance, Control and Dynamics*, *24*(6), 1225–1228.

Anderson, J. D. (1998). *Aircraft Performance and Design* (1st ed.). McGraw-Hill Education.

Bacon, B. J., & Gregory, I. M. (2007, August). General Equations of Motion for a Damaged Asymmetric Aircraft. In *AIAA Atmospheric Flight Mechanics Conference and Exhibit.*

Boeing. (2012). *Statistical Summary of Commercial Jet Airplane Accidents - Worldwide Operations 1959 - 2011* (Technical Report). Seattle, WA 98124-2207: Aviation Safety, Boeing Commercial Airplanes. Available from http://www.boeing.com/news/techissues/pdf/statsum.pdf

Finck, R. D. (1978, April). *USAF Stability and Control Datcom* (Technical Report No. AFWAL-TR-83-3048). Wright-Patterson Air Force Base, Ohio 45433: Flight Controls Division, Air Force Flight Dynamics Laboratory. Available from http://www.pdas.com/datcomrefs.html

Goman, M. G., Khramtsovsky, A. V., & Kolesnikov, E. N. (2008, April–May). Evaluation of Aircraft Performance and Maneuverability by Computation of Attainable Equilibrium Sets. *Journal of Guidance, Control and Dynamics*, *31*(2), 329–339.

Kampen, E. van, Chu, Q. P., Mulder, J. A., & Emden, M. H. van. (2007, August). Nonlinear Aircraft Trim using Interval Analysis. In *AIAA Guidance, Navigation, and Control Conference and Exhibit.*

Keller, J. D., McKillip, R. M., & Kim, S. (2009, August). Aircraft Flight Envelope Determination using Upset Detection and Physical Modeling Methods. In *AIAA Guidance, Navigation, and Control Conference.*

Kitsios, I., & Lygeros, J. (2005, August). Launch-Pad Abort Flight Envelope Computation for a Personnel Launch Vehicle Using Reachability. In *AIAA Guidance, Navigation, and Control Conference and Exhibit.*

Lombaerts, T., Schuet, S., Acosta, D. M., Kaneshige, J., Shish, K. H., & Martin, L. (2015). Piloted Simulator Evaluation of Maneuvering Envelope Information for Flight Crew Awareness. In *AIAA Guidance, Navigation, and Control Conference, AIAA SciTech.*

Lombaerts, T. J. J. (2010). *Fault Tolerant Flight Control - A Physica Model Ap-*

proach. Ph.D. dissertation, Faculty of Aerospace Engineering, Delft University of Technology. Available from http://repository.tudelft.nl/view/ir/uuid%3A538b0174-fe84-43af-954d-02f256b2ec50/

Lombaerts, T. J. J., Schuet, S. R., Wheeler, K. R., Acosta, D. M., & Kaneshige, J. T. (2013, August). Safe Maneuvering Envelope Estimation Based on a Physical Approach. In *AIAA Guidance, Navigation, and Control Conference*.

Lopez, I., & Sarigul-Klijn, N. (2010, October). A review of uncertainty in flight vehicle structural damage monitoring, diagnosis and control: Challenges and opportunities. *Progress in Aerospace Sciences*, *46*(7), 247–273.

Lygeros, J. (2003, June). Minimum Cost Optimal Control: An Application to Flight Level Tracking. In *Mediterranean Conference on Control and Automation*. Rhodes, Greece.

Lygeros, J. (2004, June). On Reachability and Minimum Cost Optimal Control. *Automatica*, *40*(6), 917–927.

Marco, A. D., Duke, E. L., & Berndt, J. S. (2007, August). A General Solution to the Aircraft Trim Problem. In *AIAA Modeling and Simulation Technologies Conference and Exhibit*.

Melikyan, A., Akhmetzhanov, A., & Hovakimyan, N. (2007, November–December). On initial value and terminal value problems for Hamilton-Jacobi equation. *Systems and Control Letters*, *56*(11-12), 714–721.

Menon, P. K., Sengupta, P., Vaddi, S., Yang, B.-J., & Kwan, J. (2013). Impaired Aircraft Performance Envelope Estimation. *Journal of Aircraft*, *50*(2), 410–424.

Mitchell, I., Bayen, A. M., & Tomlin, C. J. (2001, March). Validating a Hamilton-Jacobi Approximation to Hybrid System Reachable Set. In *Hybrid Systems: Computation and Control, Lecture Notes in Computer Science* (pp. 418–432).

Mitchell, I., & Tomlin, C. J. (2000, March). Level Set Methods for Computation in Hybrid Systems. In *Hybrid Systems: Computation and Control, Lecture Notes in Computer Science* (Vol. 1790, pp. 310–323).

NASA Aviation Safety Program. (2009, May). *Integrated Resilient Aircraft Control - Stability, Maneuverability, and Safe Landing in the Presence of Adverse Conditions* (Technical Report). Aeronautics Research Mission Directorate, NASA.

Oort, E. R. van. (2011). *Adaptive Backstepping Control and Safety Analysis for Modern Fighter Aircraft*. Ph.D. dissertation, Faculty of Aerospace Engineering, Delft University of Technology. Available from http://repository.tudelft.nl/view/ir/uuid%3A68fd89ff-aad6-4ad8-b280-d2fe8b500d48/

Oort, E. R. van, Chu, Q. P., & Mulder, J. A. (2011). Maneuver Envelope Determination through Reachability Analysis. In *Advances in Aerospace Guidance, Navigation and Control: Selected Papers of the 1st CEAS Specialist Conference on Guidance, Navigation and Control* (pp. 91–102). Springer Berlin Heidelberg.

Osher, S., & Fedkiw, R. (2003). *Level Set Methods and Dynamic Implicit Surfaces* (1st ed., Vol. 153). Springer-Verlag New York.

Ruijgrok, G. J. J. (2007). *Elements of Airplane Performance* (2nd ed.). Delft University Press.

Schuet, S., Lombaerts, T., Acosta, D., Wheeler, K., & Kaneshige, J. (2014, January). An Adaptive Nonlinear Aircraft Maneuvering Envelope Estimation Approach for Online Applications. In *AIAA Guidance, Navigation, and Control Conference, AIAA SciTech*.

Shah, G. H. (2008, August). Aerodynamic Effects and Modeling of Damage to Transport Aircraft. In *AIAA Atmospheric Flight Mechanics Conference and Exhibit*.

Stapel, J. C. J., Visser, C. C. de, Chu, Q. P., & Kampen, E. van. (2016, January). Efficient Methods for Flight Envelope Estimation through Reachability Analysis. In *AIAA Guidance, Navigation, and Control Conference, AIAA SciTech.*

Stevens, B. L., & Lewis, F. L. (2003). *Aircraft Control and Simulation* (2nd ed.). Wiley-Interscience Publication.

Stroosma, O., Smali, H., Lombaerts, T., & Mulder, J. A. (2008, August). Piloted Simulator Evaluation of New Fault-Tolerant Flight Control Algorithms for Reconstructed Accident Scenarios. In *AIAA Modeling and Simulation Technologies Conference and Exhibit.*

Tang, L., Roemer, M., Ge, J., Crassidis, A., Prasad, J. V. R., & Belcastro, C. (2009, August). Methodologies for Adaptive Flight Envelope Estimation and Protection. In *AIAA Guidance, Navigation, and Control Conference.*

Visser, C. C. de, Mulder, J. A., & Chu, Q. P. (2010, August). A Multidimensional Spline Based Global Nonlinear Aerodynamic Model for the Cessna Citation II. In *AIAA Atmospheric Flight Mechanics Conference.*

Williams, J. E., & Vukelich, S. R. (1979, April). *The USAF Stability and Control Digital Datcom, Volume I, Users Manual* (Technical Report No. AFFDL-TR-79-3032 (AD A086557)). Wright-Patterson Air Force Base, Ohio 45433: Flight Controls Division, Air Force Flight Dynamics Laboratory. Available from http://www.pdas.com/datcomrefs.html

Yi, G., & Atkins, E. M. (2010, June). Methods of Trim State Discovery. In *3rd International Symposium on Systems and Control in Aeronautics and Astronautics (ISSCAA)* (p. 654 - 659).

Zhang, Y., Visser, C. C. de, & Chu, Q. P. (2016a, January). Online Physical Model Identification for Database-driven Safe Flight Envelope Prediction of Damaged Aircraft. In *AIAA Atmospheric Flight Mechanics Conference, AIAA SciTech.*

Zhang, Y., Visser, C. C. de, & Chu, Q. P. (2016b, January). Online Safe Flight Envelope Prediction for Damaged Aircraft: A Database-driven Approach. In *AIAA Modeling and Simulation Technologies Conference, AIAA SciTech.*